COO-2564-5

BASIC RESEARCH ON CERAMIC MATERIALS FOR ENERGY STORAGE AND CONVERSION SYSTEMS

Progress Report

Donald H. Whitmore
Northwestern University
Evanston, Illinois 60201

December 1, 1978 to November 30, 1979

MASTER

December 1979

Prepared for

THE U.S. DEPARTMENT OF ENERGY
Under Contract EY-76-S-02-2564.A000

DISCLAIMER

COO-2564-5

Progress Report

covering the period from
December 1, 1978 to November 30, 1979

on

Contract EY-76-S-02-2564.A000

Basic Research on Ceramic Materials for Energy
Storage and Conversion Systems

Abstract

The present research program involves utilizing appropriate experimental probes for measuring the movement of ionic and electronic charge carriers in ceramic materials suitable for solid electrolyte and electrode applications in high-performance, secondary battery and fuel cell systems. Special emphasis is placed on developing: (1) a better understanding of the effects of structure, impurities and composition on charge carrier transport mechanisms in such materials; and (2) detailed knowledge of the kinetics and mechanism of reactions occurring (on a microscopic scale) at the electrode-electrolyte interfaces of energy storage and conversion systems.

Notice

1.1 Sodium Ion Transport Mechanisms in Layered Compounds

A recent X-ray diffuse scattering study of short-range ordering (SRO) in MgO-stabilized sodium β''-alumina ($0.9\ Na_2O\cdot 8\ MgO\cdot 5.33\ Al_2O_3$) between 77° and $750^\circ K$(1) revealed that the coherence length (a measure of the size of the ordered domains and estimated from the width of the superstructure diffuse spots) within the conducting plane saturates at about 70Å at a temperature of $280^\circ K$ and decreases with increasing temperature to about 16Å at $740^\circ K$. It has been suggested(1) that this observation is responsible for the non-Arrhenius behavior of the ionic conduction found by us and others(2-3) in the same temperature range. Assuming that the mid-temperature ($428^\circ K$) of the domain size vs. temperature plot (Ref. 1, Fig. 6) for Na β''-Al_2O_3 represents the temperature at which breakdown from single-ion, random-hopping behavior occurs on cooling, it is possible to estimate a value of the Sato-Kikuchi(4) interaction energy ϵ between a pair of nearest-neighbor Na^+ ions in the conducting slab for β''-alumina by using the exact value of the transition temperature for a two-dimensional honeycomb lattice given by Domb(5) and Rushbrooke and Scions.(6) The nearest-neighbor interaction energy, ϵ, for a Na ion pair may be derived from the exact relation

$$\exp(-\epsilon/kT_c) = 2 - \sqrt{3} = 0.267949 \tag{1}$$

when T_c is set equal to $428^\circ K$, the result is that $\epsilon \cong -0.0949$ eV ($\epsilon < 0$ implies ion repulsion between neighboring Na^+ ions). It is interesting to note that LeClaire(7) found that the variation in the Haven ratio with temperature for Na^+ ion migration in β'' and mixed phase ($\beta + \beta''$) samples was consistent with a Na^+-Na^+ nearest-neighbor interaction energy $\epsilon \approx -0.04$ eV, as roughly estimated from the Sato-Kikuchi theory.

Using our estimated value of ϵ ($\cong -0.049$ eV), it is possible to obtain a relation for the temperature-dependence of the Sato-Kikuchi product (VWf_c) for a given composition β''-Al_2O_3. Here V is the vacancy availability factor (probability of finding a vacancy next to a Na^+ ion), W the effective jump frequency factor for a Na^+ ion and f_c the correlation factor for the Na^+ ion jumps in the conduction process. Analytic expressions for V and W (but not f_c) have been given by Sato and Kikuchi in terms of the interaction energy, ϵ, and, ρ, the density of Na^+ ions within the conduction slab. Values of f_c were estimated here from the Monte Carlo results of Murch and Thorn$^{(8)}$ for ionic conduction in β''-alumina.

For our β''-crystal with $\rho = 0.92$, $\epsilon = -0.049$ eV, and an estimated transition temperature of 428°K, the temperature-dependence of the (VWf_c) product is given by

$$\begin{aligned} VWf_c &= A \exp (E/kT) \\ &= 7.41 \times 10^{-2} \exp (0.096 \text{ eV}/kT). \qquad (2) \end{aligned}$$

Because, in the present instance $\epsilon < 0$ (repulsive interaction among Na^+ ions), the interaction is expected to reduce the "true" activation enthalpy for conduction, ΔH_m, by the factor $E (= 0.096$ eV), and to make the preexponential factor σ_o smaller by the factor $A (= 7.41 \times 10^{-2})$. As Sato$^{(9)}$ has already emphasized, the effects on the activation energy and the preexponential factor are mainly due to the factor W which indicates the effect of its surroundings on the attempt frequency for the jumping Na^+ ion and the entropy factor $\exp (\Delta S_m/k)$. Applying the correction E to the apparent activation enthalpy ΔH_m^{app} observed by our β''-alumina crystal ($\rho = 0.92$), we find that:

$$\Delta H_m^{app} = \Delta H_m + E$$

$$= 0.1323 + 0.0957 = 0.2280 \text{ eV (high temperatures)}$$

$$= 0.2671 + 0.0957 = 0.3628 \text{ eV (low temperatures)}$$

TABLE I

$T^* = kT/\lvert\epsilon\rvert$	VWf_c [cal'd from Eq. (2)]	VWf_c [estimated from Sato-Kikuchi & Murch-Thorn results]
0.3	52.78	52.78
0.5	3.82	3.75
1.0	0.532	0.532

Since, for a β" crystal with given ρ, the quantity $(Nq^2a_o^2/k)$ which appears in the expression for σ_o should be constant $(= 3.805 \times 10^{-8}\ \rho)$, the expression for σ_o becomes

$$\sigma_o = (1/4)\ 3.805 \times 10^{-8}\ \rho A\nu \exp(\Delta S_m/k) \tag{3}$$

Here we have included an entropy factor, $\exp(\Delta S_m/k)$, which had not been included in the Sato-Kikuchi expression for σ_o, q the charge on the mobile cation, a_o the lattice parameter for the hexagonal cell, k the Boltzmann constant, ν the attempt frequency for the Na^+ ion jump and ΔS_m the entropy change associated with a Na^+ ion jump. Solving Eq. (3) for the product $\nu \exp(\Delta S_m/k)$ and substituting therein the σ_o values derived from our experimental observations, the A value from Eq. (2) and the measured ρ value = 0.92, we find that

$$\nu \exp(\Delta Sm/k) = 1.0514 \times 10^8\ \sigma_o/A\rho$$

$$= 1.5367 \times 10^9\ \sigma_o \tag{4}$$

For the high-temperature conductivity region exhibited by our β''-alumina sample, $\nu \exp(\Delta Sm/k) = 6.252 \times 10^{12}$ Hz while, for the low-temperature region, $\nu \exp(\Delta Sm/k) = 2.055 \times 10^{14}$ Hz. Assuming that the energy barrier for Na^+ ion jumps is sinusoidal, we can write for the attempt frequency, ν,

$$\nu = [\ 3\Delta H_m^{app}/2a_o^2M\ ]^{\frac{1}{2}} \tag{5}$$

where M is the mass of the mobile ion and ΔH_m^{app} the apparent enthalpy of motion of the mobile ion. At low temperatures, the ν value for Na^+ ion motion estimated by means of Eq. (5) is 2.31×10^{12}Hz, whereas at high temperatures the value is 1.63×10^{12}Hz. A reasonable comparison can be made between our high-temperature value (1.63×10^{12} Hz) and the ν value found by Bates et al.(11) from the Raman peak occurring at 33 cm^{-1} ($\approx 1.0 \times 10^{12}$ Hz), despite the crudeness of our estimate of the attempt frequency.

Thus, it is reasonable to assume that, at high temperatures, $\sigma_o = 123.32\nu(cm)^{-1}$ where ν is the attempt frequency, taken to be the 33 cm^{-1} value given by Bates et al.(11) This σ_o value, it is noted, is about 3 times larger than the Bates' random-walk σ_o value for sodium β''-alumina. Using Bates' attempt frequency value, the value of $\exp(\Delta S_m/k)$ in the high-temperature region is estimated to be 6.252 and thus $\Delta S_m = 1.60 \times 10^{-4}$eV/deg. Similar calculations of the factors $\exp(\Delta S_m/k)$ and ΔS_m in the low-temperature regime yield 2.055×10^{14} Hz and 3.87×10^{-4}eV/deg., respectively, using a value for $\nu(= 2.312 \times 10^{12}$Hz) estimated from Eq. (5).

Based on their X-ray diffuse scattering results for sodium β-alumina, McWhan et al.(10) concluded that an increase in the size of the SRO domains (as measured by the coherency length) inhibits ionic conductivity and results in a breakdown of the single-ion, random-hopping behavior, as inferred from far infrared and tracer diffusion data on this material. Similar inhibition of the ionic conductivity (but even more pronounced because of the larger ordered domain sizes encountered) should be expected in sodium β"-alumina when ordering sets in at temperatures below 500°K. Furthermore, O'Keefe has suggested that the pre-exponential factor, σ_o, in the Arrhenius conductivity expression should increase relative to the random-hopping value in the presence of a cooperative mechanism of diffusion; this is consistent with the predictions of the Sato-Kikuchi model$^{(4)}$ and also accords with our observation for sodium β"-alumina that the low-temperature σ_o value is appreciably larger than the high-temperature value.

Finally, the self-diffusion findings of Lazarus et al.$^{(12)}$ on the Cs-Cl type β-brass (50 Cu:50Zn) superlattice revealed that the atomic diffusion coefficients were significantly smaller when the host material was in a highly long-range ordered state than when long-range was absent. The temperature-dependence of the atomic diffusion coefficient was non-Arrhenius in nature and resembled the two-slope behavior found here for Na^+ ion conduction in the β"-alumina. The atomic diffusion data for the ordered state for this Cu-Zn alloy can be rationalized on the basis of a six-jump vacancy cycle discussed by Elcock and McCombie$^{(13)}$; this mechanism allows diffusion to occur by means of nearest-neighbor vacancy jumps and, after completion of the cycle, the vacancy has been found to move a given distance while the long-range order of the system is still preserved.

Similarly, a cycle of vacancy jumps which would leave the degree of ordering unchanged, could be invoked in the case of Na^+ ion jumps in the ordered (low-temperature) state of β"-alumina. The entropy of migration for such a jump cycle in the ordered state would be expected to be larger than that expected by single-ion, random hopping behavior prevalent at high-temperatures; indeed, this expectation was realized in our Na^+ ion conductivity data as well as that of Farrington and Briant(3) and Cole et al.(14)

Other inferences possible from a comparison of the present high-temperature conductivity results on sodium β''-alumina crystals ($\rho \cong 0.84$) in the same temperature regime are: (1) the true enthalpy of migration values ΔH_m are essentially identical ($\approx 0.228 - 0.230$ eV) for the two different compositions; (2) the ratio of the attempt frequencies for the two sets of data should be proportional to the square root of the ΔH_m^{app} ratio ($= \sqrt{0.12/0.13} = 0.96$) (3) the ratio of the pre-exponential factors (σ_o) should be proportional to the ratio of the product ($A\rho\nu$) and this expectation is closely obeyed; and (4) as might be expected, the factor A in Eq. (2) should scale roughly as ($1-\rho$), the site fraction of Na^+ ion vacancies in the conduction slab.

1.2 Conductivity and Dielectric Constant Measurements on Sodium β''-Alumina at Microwave Frequencies

During the past year, a modest research effort was started in collaboration with Professor M. Brodwin (Department of Electrical Engineering) which had as its goal the evaluation of the frequency-dependence of the ionic conductivity and dielectric constant of some model solid electrolytes in the microwave and the infrared frequency regimes. Our ultimate intention here is to prepare samples and characterize the ionic transport behavior of selected solid electrolytes exhibiting either two- or three-dimensional pathways for the mobile ion by observing the aforementioned properties over the microwave range 0.1 to 140 GHz and also over the infrared range 200 GHz to 300 THz. The main objective for this study is to extend our basic understanding of the detailed microscopic and dynamical behavior of the mobile ions in ceramic fast ion conductors.

Our initial experiments were carried out by H. Kafka, a senior Electrical Engineering student, on ceramic sodium β''-alumina at a single microwave frequency (24 GHz) over the temperature range 20° to 440°C. The data was obtained by means of a short-circuited line method with the sample contained in a heated stainless steel, rectangular waveguide.

The real part of the Na^+ conductivity at 24 GHz of the β''-alumina sample ranged from 9.7×10^{-2} $(\Omega\ cm)^{-1}$ at 25°C to 5.0×10^{-1} at 220°C (see Fig. 1). At still higher temperatures, the ionic conductivity appears to decrease. Over the range of temperature from 25° to 220°C the activation energy for conduction is 0.14 eV, comparable to that observed for low-frequency observations of the bulk conductivity of this material.

The real part of the dielectric constant of sodium β''-alumina, measured at 24 GHz, decreased as the temperature was increased, passed through zero and then became negative (see Fig. 2). The room-temperature value of the dielectric constant was about 21 and the zero cross-over point, occurring at about 340°C, corresponded to the maximum in the $\ell n(\sigma' T)$ vs. T^{-1} curve. As has been shown by the earlier microwave observations on the copper and silver ion solid electrolytes, in the temperature range where negative values of ϵ' are encountered, σ' decreases in magnitude and takes on increasingly smaller values the more negative ϵ' becomes. While such behavior is totally consistent with predictions based on a Drude-like model for the fast ion conduction process, additional microwave observations of σ' and ϵ' at several other frequencies will be required before a proper theoretical interpretation of the mechanism of Na^+ ion motion in the β''-alumina structure is likely to emerge.

1.3 Effects of Impurities on Ionic Conductivity in Sodium β''-Alumina

Calcium is a common impurity present in the starting materials such as

$LiNO_3$, Na_2CO_3, etc. which are commonly employed in the fabrication of sodium β"-alumina. Accordingly, a study of the effect of Ca impurities on the ionic conductivity of sodium β"-alumina is important technologically as well as representing a very interesting and challenging scientific problem because there are several possible locations for the Ca^{2+} ions in the β"-alumina lattice and each should have its own effect on the resulting ionic conductivity. For instance, it is possible that:

(1) Ca^{2+} may occupy the vacant Na^+ ion sites on the conduction planes and it may also form a dipolar complex with a near-neighbor sodium vacancy, both possibilities leading to a decrease in the bulk Na^+ ion conductivity;

(2) Ca^{2+} may also be segregated, or even precipitated as a Ca-rich second phase, at/or near the grain boundary and form a nonconductive layer in such locations, thereby decreasing the grain boundary conductivity.

Table I lists some of the physical properties of the CaO-doped samples. It is apparent that the conversion to the β" phase in this case of the doped samples is very poor, implying that the presence of Ca^{2+} ions inhibits or partially nullifies the effectiveness of Li_2O as a stabilizer in β"-alumina. However, there is no simple connection between the amount of CaO present in the β"-alumina sample and its percentage of conversion to the β" phase. It should also be noted from the data of Table I that the presence of calcium appears to enhance the densification process during sintering. Jones and Miles(14) reported that an addition of Ca to β-alumina enhances sintering and permits densification below 1750°C.

Typical B vs. G plots at different temperatures for a Na β"-alumina sample, doped with 0.7 wt% CaO, are shown in Figures 3 to 6. Due to the change in value of those circuit parameters affected by the presence of CaO, the shape of the complex-plane plots shifts towards the low-frequency end; i.e., in order to see a complete polarization arc, it is necessary to extend the measurements to higher frequencies than were required for the undoped samples. The method for deriving of circuit parameters from complex-admittance plots was detailed in earlier Progress Reports.

Figure 7 shows an isothermal conductivity-composition plot for bulk conductivity at 300°C. The dependence of the bulk conductivity, σ_b on the composition of CaO-doped samples appears to be adequately described in the form $\log \sigma_b = -mx + \log \sigma_p$, where σ_p is the bulk conductivity of an undoped sample, x is the wt% of CaO doped and m is a constant. This relation is very similar to the logarithmic mixing rule used for conductivity when a layered model for a multiphase system is treated, viz., $\log \sigma = \sum_i V_i \log \sigma_i$ where V_i is the volume fraction of the i^{th} layer and σ_i is its partial conductivity. This relationship implies that Ca^{2+} ions penetrate onto the conduction planes and form regions of lower conductivity. An NMR study of the motion of ^{23}Na in β-alumina doped with Ca was reported by Roth(15) in which he found that Ca^{2+} ions are incorporated as a solid solution with Na^+ ions on the conduction plane, forming regions with the magnetoplumbite structure.

Hsieh and DeJonghe(16) also reported the relation between the bulk conductivity for the SiO_2-doped Na β-alumina electrolyte and the silica content of the compound. Their results also obeyed the logarithmic mixing rule mentioned above. These investigators concluded that the formation of increasing amounts of glassy sodium aluminosilicates and α-alumina in the β-alumina electrolyte was responsible for the observed decrease in bulk conductivity as the amount of SiO_2 was increased. In order to explain the degradation of the bulk conductivity which occurs when the Na β''-alumina is doped with Ca, it is important to recognize that Ca^{2+} ions occupying Na^{+} ion sites on the conduction plane might affect the bulk Na^{+} ion conductivity in two ways: (1) a Ca^{2+} ion, on occupying a near-neighbor cation vacant site to a jumping Na^{+} ion, lowers the probability of a Na^{+}-vacancy exchange occurring for that ion; and (2) there is a likelihood that dipolar complexes can form between a Ca^{2+} impurity ion and a neighboring vacancy on the conduction plane.

Based on experience with doped alkali halide systems, it would be expected that the cation vacancies bound in such complexes would exchange positions with jumpting Na^{+} ions more slowly than would unassociated cation vacancies. Both of these possibilities will certainly impede the mobility of Na^{+} ions in the bulk phase.

Figure 8 shows log $\sigma_b T$ vs. T^{-1} plots for Na β''-alumina samples doped with different amounts of CaO. From this figure, it is apparent that the slope for the Arrhenius conductivity-temperature plots becomes larger as the CaO concentration of the sample increases. It is interesting to note that, in the case of 1 wt% CaO-dopant in a Na β''-alumina sample, the activation energy for bulk Na^{+} ion conduction reaches about 0.49 eV, thereby rendering this material no longer very suitable as a superionic conductor. Although the addition of 1 wt% CaO to β''-alumina does not cause the 50- to 100-fold decrease in conductivity which was found for β-alumina, nevertheless it does seriously degrade the performance of β''-alumina as an electrolyte in a Na-S cell. While some of the observed decrease in ionic conductivity of the doped samples, when compared with "pure" β''-alumina, may be attributable to the incomplete conversion to β''-phase in the doped material, this factor alone cannot entirely account for a decrease of about 10-fold in the bulk conductivity.

Figure 9 shows an isothermal conductivity-composition plot for grain boundary conductivity for the CaO-doped Na β"-alumina samples at 106°C. Determination of the grain boundary conductivity really depends upon the microstructure of each sample. Rigorous comparisons among samples doped with different levels of CaO are difficult, even though the sintering and annealing procedures are presumably the same. Nevertheless, it was observed that the relation between the conductivity of doped and undoped samples again approximately obeys the logarithmic mixing rule. Error bars were used in Figure 9 to indicate the experimental uncertainties that are expected to arise because of variations in the microstructure as well as in other factors. The grain boundary conductivity of doped samples shows a much more pronounced dependence on the concentration of CaO than it does the bulk conductivity.

It is noteworthy that the activation energy for grain boundary conduction in CaO-doped samples increases slightly with the concentration of CaO, changing from 0.32 to 0.43 eV for a variation in doping level from 0.05 to 1 wt% CaO. The grain-boundary capacitance results on CaO-doped samples should provide further insight into the effects of Ca-doping of Na β"-alumina. As shown in Figure 10, the grain boundary capacitance decreases substantially with increasing CaO content but does not follow a linear relationship. Since the capacitance of a nonconductive layer is a linear function of the thickness of that layer, the observed non-linear relationship between grain boundary capacitance and the CaO-doping level indicates that segregation of Ca^{2+} to the grain boundary regions is more likely than is a uniform distribution of Ca within the polycrystalline sample.

Direct observation of a possible segregation of calcium to the grain boundaries was accomplished with the aid of a scanning Auger spectrometer. Figure 11 shows an Auger map for the element Ca of a Na β''-alumina sample doped with 1 wt% CaO. Auger mapping is a technique which records the distribution of a selected element by employing the intensity of the collected Auger electrons as a function of the concentration of an element in a finite area.

The calcium Auger mapping was performed on an as-cut sample, and the result shown in Figure 11 indicates segregation of Ca along the grain boundaries. Use of an as-cut sample in this study allowed direct observation of this segregation with the Auger-mapping technique. In contrast, if a fracture-surface was examined, the Auger mapping of calcium would yield nearly uniform intensity over the entire area examined since, with an intergranular fracture, all of the grain boundaries are exposed to the Auger probe on the fractured surface. A typical Auger spectrum is shown in Figure 12. Surprisingly, no major peaks attributable to impurities were detected on the as-cut surface, except for that due to carbon. The characteristic peaks used for identification and analysis purposes are: O(504 eV), Ca(291 eV), Li(58 eV), Al(68 eV), C(272 eV). Figure 12 shows that all of these peaks shift to lower energies due to the "surface-charging effect" of the specimen even though the samples were sputtered-coated with very thin layers of gold (~ 5Å thick). A discoloration of the specimens was observed and that can likewise be attributed to surface-charging effect.

A chemical analysis method was employed to estimate the approximate concentration of Ca existing at the grain boundaries and this result could then be compared with that assuming Ca is uniformly distributed throughout the specimen. Such a comparison should enable one to decide whether Ca is segregated to the grain boundary regions. The relative peak-to-peak heights of the Auger peaks shown in Figure 12 for O, Al, and Ca are in the ratio O : Al : Ca = 78.6 : 14 : 9. The atomic concentration for element X, C_x, can be calculated by using the following equation:(17)

$$C_x = \frac{\dfrac{I_x}{S_x\ d_x}}{\sum_i \dfrac{I_i}{S_i\ d_i}} \qquad (6)$$

where I_x is the peak-to-peak amplitude of the element X in the Auger spectrum from the test specimen, d_x the scale factor, S_x the relative sensitivity between any element, X, and silver. By using the tabulated data(17) for Al, O, and Ca [$S_{Al} = 0.24$, $S_O = 0.5$, $S_{Ca} = 0.45$ and $d_{Al} = d_O = d_{CA} = 1$], the atomic ratios, calculated with the aid of Eq. (6) are: l.c

O : Al : Ca = 100 : 37(± 11) : 12.7(± 2)

This result may how be compared with the ratio expected on the basis of known sample composition and the assumption of a uniform Ca distribution; vis., the normalized atomic ratio O : Al : Ca = 100 : 62 : 0.63 can be calculated from the starting composition: 1 wt% CaO, 8.85 wt% Na_2O, 0.75 wt% Li_2O, and 89.4 wt% Al_2O_3. The ratio, estimated using Eq. (6), may be somewhat uncertain as a result of : (a) the slightly different operating conditions between our experiments and those used in obtaining the data tabulated in the Auger handbook; (b) the characteristics of instruments used (principally, the detectors and lock-in amplifier); and (c) the roughness of the sample surface. In spite of these sources of uncertainty, the ratio calculated from the present observations is believed to constitute a strong indication that the concentration of calcium at the grain boundaries is at least 10 times larger than that within the grains.

An estimation of the thickness of the Ca-enriched layer was undertaken using ion-milling. The point analysis of the Auger spectrum on a 0.7 wt% CaO-doped Na β"-alumina sample is shown in Figure 13 where it is clearly evident that the height of argon (215 eV) peak increases as the sputtering time increases, implying that there may be some argon atoms embedded in the sample surface. On the other hand, the height of Ca (291 eV) peak and carbon (272 eV) peak diminished after sputtering for 15 min. The removal rate of sample surface with the electron gun of the instrument operated at 2 kV and 25 mA was estimated to be 20 to 30 Å/min. On the basis of these results, the thickness of the Ca-enriched layer was estimated to be 300 to 450 Å.

In summary, then, the presence of Ca^{2+} ions in the Na β"-alumina samples, even at low concentration (⩽ 1 wt% CaO), was found to have a detrimental effect on both the bulk conductivity and the grain boundary conductivity, with the effect being more severe in the case of the grain boundary conductivity. Moreover, the grain boundary capacitance decreased substantially as the CaO-content increased. Segregation of Ca near or at the grain boundaries of the sample forming a Ca-rich, nonconductive layer was invoked to explain the behavior of these properties with CaO-doping. Scanning Auger microscopy confirmed that, indeed, segregation of Ca did occur at the grain boundaries of β"-alumina.

2. Alkali Ion Transport in Three-Dimensional Fast Ion Conductors

To date, the most promising solid electrolytes for the Na-S cell have been β and β"-alumina; however, because of their layered nature these compounds exhibit highly anisotropic thermal expansion coefficients$^{(18)}$ which often cause several internal stresses in sintered membranes during thermal cycling which may lead to membrane failure. Moreover, the confinement of the mobile sodium ions to widely separated layers sharply reduces the fraction of membrane volume that contributes to ionic conduction.

Recently, there has been much interest in a new class of compounds known as skeleton structures. Sodium antimonate and NASICON ($Na_3Zr_2Si_2PO_{12}$) are such skeletal compounds and they consist of a rigid subarray with intersecting tunnels in which the alkali ions can move in three dimensions, thereby alleviating the problems associated with the two-dimensional, layered compounds. While sodium antimonate has not yet been employed as the electrolyte in any practical cell, it is scientifically interesting because it displays both chemical and structural variability and is the only compound of its class that has been studied in both the single and polycrystalline form.

2.1 Sodium Ion Transport in the Cubic Antimonate $NaSbO_3 \cdot \frac{1}{6}\,NaF$

Sodium antimonate ($NaSbO_3$) exists in two forms: ilmenite and body-centered cubic. Only the cubic form exhibits rapid ionic transport and is synthesized from cubic potassium antimonate via ion exchange.

The compound $KSbO_3$ can be synthesized in both a primitive cubic and body-centered cubic form. Both structures have the same framework consisting of edge-shared SbO_6 octahedra, forming Sb_2O_{10} clusters, that are connected by shared corners. Tunnels consisting of face-shared octahedral sites of two distinct types (M1 and M2) traverse the skeleton in $\langle 111 \rangle$ directions, intersecting at body-centered positions. Potassium ions occupy M1 and M2 sites only; this occurs in an ordered manner in the primitive cubic form and in a disordered fashion in the b.c.c. form.(19,20) A schematic representation of the arrangement of M1, M2, and body-centered (BC) sites is shown in Figure 14. There are twenty-four M1, M2 sites (half of which are occupied by K^+) and two body-centered sites per unit cell.

The only known method of synthesizing "pure" $KSbO_3$ in the cubic forms is by means of high pressure(21) (greater than 20 kb) applied at high temperature (~ 700°C). However, Brower et.al.(22-24) have discovered a means of fabricating b.c.c. and primitive cubic $KSbO_3$ at ambient pressure by inserting a monovalent anion into the body-centered position. Insertion of the OH^- ion stabilized the primitive cubic form, whereas, insertion of the F^- ion stabilizes the body-centered cubic form.

The structural formula for the anion-stabilized potassium antimonate is

$$[\,\square_2 L_{14} X_2\,]^{12+}[\,Sb_{12}O_{36}\,]^{12-}$$

where $\square$ denotes a vacant cation site and X represents a hydroxyl anion or a fluoride ion. The common chemical representation for the fluorine-stabilized antimonate corresponding to the above structural formula is $KSbO_3 \cdot \frac{1}{6}(KF)$ which has a b.c.c. structure. The structural formula indicates that the anion stabilized antimonate is non-stoichiometric.

Brower et.al.(23,24) have also reported that monovalent anions (OH^-,F^-) can substitute for oxygen on the octahedral framework. Such a substitution requires charge-compensation which occurs by removal of cations. The structural formula then becomes:

$$[\,\square_{2+y} K_{14-y} X_2]^{(12-y)+}[Sb_{12}O_{36-y}X_y]^{(12-y)-}$$

where y has been reported to be as large as three.

The potassium ion in $KSbO_3 \cdot \frac{1}{6}(KF)$ can be ion exchanged for Li, Na, Rb, and Ag.(21,22) There has been only one reported investigation of sodium ion exchange of hydroxyl-stabilized potassium antimonate.(22) Curiously, while hydroxyl-stabilized potassium antimonate is primitive cubic (i.e. ordered K^+ ions), the sodium analog has a b.c.c. structure (i.e. disordered Na^+ ions). Table II summarizes the various methods of synthesis of b.c.c. and primitive cubic antimonates.

Goodenough et.al.(19,20) reported that fine $NaSbO_3 \cdot \frac{1}{6}(NaF)$ powder can be hot-pressed to greater than 95% of theoretical density at 30,000 psi and a temperature of 600°C in a vacuum if two weight percent $NaNH_2$ is added to the powder. A similar method will be used to obtain dense samples.

Single crystals have been grown in our laboratories by suspending pressed pellets of $NaSbO_3 \cdot \frac{1}{6}(NaF)$ over molten NaF at 1275°C for four hours as shown in Figure 15. The crystals are embedded in a fine grained matrix usually consisting of a compound with a pyrochlore structure and can be easily separated from the matrix material. The largest crystals (~ 1 mm) are found in the center of the compact and are well-formed, truncated cubes. Micrographs 1 and 2 show typical crystals.

Brower et.al.(24) have been able to produce one millimeter size $NaSbO_3 \cdot \frac{1}{6}NaF$ crystals by heating a $NaF\text{-}Sb_2O_4$ mixture (molar ratio 93:7) at 1250°C for 35 minutes.

Characterization of polycrystalline samples will include quantitative stereology, SEM, X-ray diffraction, and density determination via an immersion technique based on Archimedes' principle.

The only reported ionic conductivity studies have been performed on the body-centered cubic $NaSbO_3$ fabricated at high pressure(20) and the fluorine-stabilized sodium antimonate, $NaSbO_3 \cdot \frac{1}{6}(NaF)$.(20,25) Goodenough, Hong and Kafalas(20) have found that placement of fluorine atoms at tunnel intersection sites (BC sites) does not hinder sodium ion transport, suggesting that sodium ions can jump from one M1 sites to another without passing through the BC site. They note that this observation agrees with the anomalously large temperature coefficient for sodium ions in M1 sites which indicates that thermal motion along $\langle 100 \rangle$ directions is about six times larger than that along $\langle 111 \rangle$ directions.

There are some differences between the ionic conductivity data of Goodenough et.al.(20), Singer et.al.(25) and the results obtained in our laboratory. Goodenough and coworkers(20) have reported an activation energy of about 0.35 eV for ionic conductivity measurements made on polycrystalline $NaSbO_3 \cdot \frac{1}{6}(NaF)$ using graphite electrodes and a frequency of 1000Hz. Singer et.al.(25) have reported an activation energy of about 0.45 eV for dc measurements on polycrystalline $NaSbO_3$ and $NaSbO_3 \cdot \frac{1}{6}(NaF)$ using reversible electrodes ($NaNO_3$ or $NaPF_6$ in propylene carbonate). A.C. conductivity studies performed in our laboratory on single crystal $NaSbO_3 \cdot \frac{1}{6}(NaF)$ with graphite electrodes yielded a low-temperature (less than $300^{\circ}C$) activation energy of between 0.46 eV and 0.49 eV and a high-temperature activation energy of between 0.34 eV and 0.38 eV (see Figure 16).

While the data of Singer et.al.(25) agrees with our results between $25^{\circ}C$ and $300^{\circ}C$, Goodenough's results are significantly different. The discrepancy may lie in the fact that Goodenough et.al.(20) used single frequency 1 kHz data which can easily lead to error. A replot of Goodenough's original data is given in Figure 17 and clearly shows a two-slope behavior.

The high-temperature slope in this replot yields an activation energy of about 0.46 eV, in good agreement with the present results and those of Singer et.al. However, the low-temperature slope indicates an activation energy of about 0.29 eV, which may be an artifact of their measuring technique. Specifically, measurements like Goodenough et.al's are reliable only so long as the process of interest, in this case bulk conduction, is the primary cause of the overall impedance. Ionic transport through the bulk usually dominates the overall impedance at high temperature, but at low temperatures other processes such as double-layer polarization, grain-boundary polarization and transport, and geometric capacitance are more likely to contribute to the overall impedance. In summary, then, if the low-temperature data of Goodenough et.al. is disregarded, then the activation energies and magnitudes of the observed ionic conductivity found by the three groups are in good agreement (see Figure 18).

Our ac conductivity measurements indicate that a process with an activation energy of about 0.34 eV was rate-determining at high temperatures, suggesting that this process occurs in series with ion transport through the bulk. An understanding of the nature of this high-temperature activated process requires an understanding of ac conductivity. The complex admittance $Y(\omega)$ can be expressed as the sum of the conductance $G(\omega)$ and susceptance $B(\omega)$:

$$Y(\omega) = G(\omega) + iB(\omega)$$

Similarly, the complex impedance is the sum of the resistance $R(\omega)$ and reactance $X(\omega)$; viz.:

$$Z(\omega) = \frac{1}{Y(\omega)} = R(\omega) + iX(\omega)$$

A plot of the imaginary vs. real part of the admittance or impedance has distinctive features, characteristic of certain combinations of circuit elements. Analysis of $B(\omega)$ vs. $G(\omega)$ and $R(\omega)$ vs. $X(\omega)$ plots, in combination with some knowledge of the physical processes occurring in the system, allows one to construct a so-called equivalent circuit.(26) Each element of the equivalent circuit (usually resistors and capacitors) can be associated with a particular physical process such as double-layer capacitance, grain-boundary resistance and capacitance, bulk resistance, or an interfacial reaction polarization.

Another powerful tool used in the construction of equivalent circuits is the Bode diagram which plots log impedance Z vs. log frequency ω. Figure 19 is a typical Bode plot for a $NaSbO_3 \cdot \frac{1}{6}(NaF)$ single crystal with graphite electrodes. Note how the overall impedance is determined by different physical processes at different frequencies and temperature. The plateau regions are typical of purely resistive processes, whereas, regions of unit slope are characteristic of polarization within the electrode-electrolyte system.

Based on admittance (impedance) and Bode plots, the following equivalent circuit can be constructed for $NaSbO_3 \cdot \frac{1}{6}(NaF)$ single crystals with graphite electrodes.

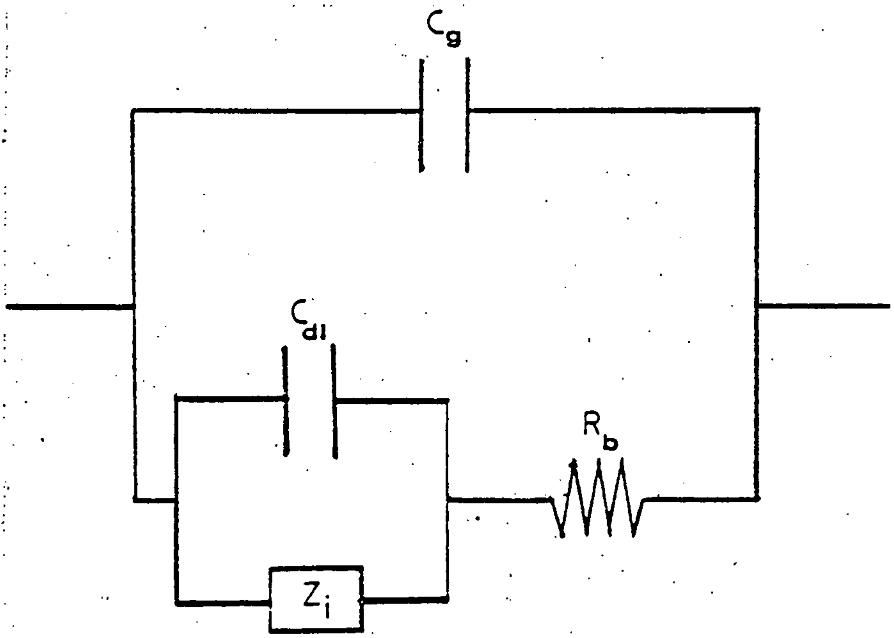

FIGURE 20. Equivalent circuit for $NaSbO_3 \cdot \frac{1}{6}(NaF)$ with graphite electrodes.

Here C_g and C_{dl} are the geometric and double capacitances, respectively, R_b is the bulk resistance and Z_i is a complex interfacial impedance likely involving a charge transfer reaction and diffusion of sodium into the graphite electrodes. The experimentally-determined values for each element are given in Table III. The solid curves in Figure 19 represent calculations based on the equivalent circuit shown in Figure 20.

The equivalent circuit seems to indicate that the high-temperature activated process shown in Figure 16 occurs at the electrode-electrolyte interface, probably involving a charge-transfer reaction.

2.2 Sodium Ion Transport in NASICON ($Na_3Zr_2Si_2PO_{12}$)

It has been demonstrated recently that materials with the general composition $Na_{1+x}\,Zr_2\,Si_xP_{3-x}O_{12}$ $(0.4 \leq x \leq 2.8)$ are among the best fast Na^+ ion conductors currently available.$^{(27-29)}$ A maximum in the ionic conductivity is found for x = 2, i.e., at the NASICON composition, $Na_3Zr_2Si_2PO_{12}$. At 300°C, this compound exhibits a Na^+ ion conductivity comparable with that found in sodium β-alumina. Moreover, NASICON has been shown to be stable when in contact with liquid sodium and sulfur at 350°C. Accordingly, it has considerable promise as the solid electrolyte in the Na/S batteries.

The observed high mobility of Na^+ ions in this compound occurs by Na^+ ion transport through tunnels in a rigid network made up to SiO_4 and PO_4 tetrahedra sharing corners with ZrO_6 octahedra. At room temperature, $Na_3Zr_2Si_2PO_{12}$ crystallizes with monoclinic symmetry (space group $C_{2/c}$), but this transforms on heating at about 152°C (425°K) to a phase with rhombohedral symmetry (space group $R\bar{3}c$).$^{(30,31)}$ Thus, at the operating temperature of the Na/S cell (≈ 350°C), the rhombohedral form of NASICON is the stable one and its properties and an understanding thereof are of primary interest in this study.

NASICON specimens were prepared by taking weighed amounts of Na_2CO_3, $NH_4H_2PO_4$, ZrO_2 and SiO_2, apportioned in the ratio 0.2842 : 0.1795 : 0.3847 : 0.1876 (respectively) mixing these for 2h in a vibratory mill using stabilized zirconia balls and a heptane solvent. The mixed powder was dried, calcined in a zirconia crucible at 1150°C for 16h, then ball milled again for 1.5h, followed by drying. Cylindrical pellets were prepared by first pressing the ground powder in a die at $\approx$ 2kbar and then isostatically pressing the resulting pellet at $\approx$ 4kbar. The pellet was subsequently sintered in air at 1250°C for 8h.

All sintered specimens were polished with diamond paste to a 1 μm finish and a density determination was then made by weighing before and after immersion in heptane (Archimedes' method). The densities resulting from the foregoing preparatory method were 97 to 98% of the theoretical value (estimated to be 3.27 g cm^{-3} from Hong's X-ray data on the monoclinic structure (27)).Open porosity was found to be negligible in these highly dense samples. X-ray diffraction patterns were routinely made on each batch of specimens, using CuK_α radiation and Philips diffractometer operated at a scanning rate of one degree in 2θ per min. The resulting powder pattern was compared with the calculated pattern (obtained using the LAZY-PULVERIX computer program) from Hong's data. All major peaks in the 2θ range between 13° and 35° were identified and indexed (both with respect to peak position and relative intensity) before proceeding with a conductivity measurement.

Three kinds of electrodes were used on conductivity specimens: sputtered gold, sputtered platinum or graphite. The first two of these are ion-blocking, whereas graphite may be quasi-reversible with respect to Na^+ ions.(19) The specimen was heated in vacuum at 300° C for 2h and conductivity measurements were made under a dry argon atmosphere at 20° to 30° intervals during cooling down to room temperature. The automatic frequency response analyzer, which was designed and built in our laboratories, was employed to obtain the complex admittance (or impedance) data.

Conductivity values were obtained from the intercept of the high frequency polarization arc with the real (G) axis of the admittance plot. Figure 21 is a typical Arrhenius plot of $\ell n\ \sigma T$ vs. T^{-1} for one of our NASICON specimens and shows two distinct conductivity regions: one below about 410°K (monoclinic phase) with an activation energy of 0.331 eV and the other above approximately 450°K (rhombohedral phase) with an activation energy of 0.182 eV. The conductivity region between 410° and 450°K represents a transition region in which the phase transformation from the monoclinic form of NASICON to the rhombohedral form is occurring.

These low-frequency (up to 700 kHz) conductivity will soon be extended to frequencies of the order of 100 MHz as a prelude to extending our conductivity results to still higher frequencies (into the microwave and optical frequency ranges).

3. Enhancement of Ionic Transport in Solid Electrolytes Arising from the Presence of Inert, Second-Phase Particles.

About six years ago Liang (Mallory Battery Co.) made the interesting discovery that the incorporation of finely-divided, seemingly inert aluminum oxide particles into LiI greatly enhanced ion conductivity (10^{-5} $(\Omega\ \mathrm{cm})^{-1}$ at 298°K). Liang observed that a classical doping mechanism could not be responsible for this enhancement since the maximum effect occurred for additions of 50 to 60 mole percent Al_2O_3 which is well above the solubility limit ($<$ 2 mole %), and he suggested that the creation of Li^+ ion vacancies by the dissolution of surface aluminum oxide molecules into the LiI near the interfaces might be responsible for the enhancement observed. Since Liang's discovery, space-charge models, models involving formation of highly conductive layers around each inert particle or postulates that water plays a role in the enhancement have been put forth. None of these ideas is completely satisfactory and we now believe that a dislocation model, which is detailed in this year's renewal proposal, is a more realistic way of accounting for Liang's observations. The results of the early phase of our program to test the validity of our model are described below and future experiments along these lines are outlined in this year's proposal.

The study of the LiI + SiO_2 (inert phase) system requires strict control of impurity content (both anion and cation), water content, grain size and SiO_2 particle size. The past few months have been spent setting up the controlled atmosphere apparatus and characterization of the LiI and SiO_2.

Initial studies of rather impure LiI indicated that a sharp jump in the ionic conductivity of nearly two orders of magnitude occurred near 185°C. The intrinsic and extrinsic activation energies of 0.96 eV and 0.44 eV, respectively, compare well with those reported in the literature, but there have been no reports of a large increase in conductivity at 185°C. Careful examination of the data of Ginnings and Phipps(32), however, shows a small "bump" in the conductivity at about 185°C.

Jackson and Young(33) note that the trihydrate of LiI cannot be dehydrated above its melting point of 63°C without decomposition. This statement led to the speculation that a significant amount of LiOH could be present in the dehydrated LiI, depending on the amount of trihydrate initially present and the dehydration procedures.

The LiI-LiOH system has a eutectic temperature of about 180°C. To help confirm the presence of LiOH in dehydrated LiI, the conductivity of a mixture of about 50 m/o LiI and 50 m/o LiOH was measured over the temperature range 20°C to 500°C. Figure 22 compares the conductivity of the LiI-LiOH mixture to that of dehydrated LiI. It is readily seen that the mixture has an Arrhenius plot which is similar in many respects to that for the dehydrated LiI.

The "excess" conductivity, then, is most likely due to the formation of liquid phase at 185°C which provides a short-circuiting path through the sample. A series of LiI-LiOH mixtures have been prepared and await further study.

It should be noted that Liang's original patent on the LiI + Al_2O_3 system states that LiI-LiOH mixtures are suitable for the matrix phase. In addition, Biefeld and Johnson(34) have found a sharp increase in conductivity for Li_2SO_4-LiOH mixtures at 350°C which is the eutectic temperature for the system.

The equivalent circuit for the circuit for pure LiI is complex. It involves a diffusional impedance (Warburg) which is detectable at high temperatures, a geometric and a double layer capacitance, a bulk resistance and a second resistive element possible involving charge transfer. To date, we have not formulated the arrangement of the elements of the equivalent circuit.

The Warburg impedance may be due to the diffusion of a neutral species (I_2) through LiI, perhaps along grain boundaries. This hypothesis is consistent with observations by Armstrong et.al.(35) of the Pt/Ag_4RbI_5 system and with the slight pinkish color of the salt after their measurements had been made. The charge transfer may involve the following reactions

$$I^- \rightleftarrows I^\bullet + e$$

$$I^\bullet + I^- \rightarrow I_2 + e$$

as discussed by Armstrong et.al.(35)

REFERENCES

1. G. Collin, Ph. Colomban, J. P. Boilot and R. Comes, in Fast Ion Transport in Solids, ed. by P. Vashishta, J. N. Mundy and G. K. Shenoy (New York: Elsevier North-Holland,Inc., 1979) p. 309.
2. J. T. Kummer, in Progress in Solid State Chemistry, ed. by H. Reiss and J. O. McCaldin (Oxford: Pergamon Press, 1972) p. 141.
3. G. C. Farrington and J. L. Briant, in Fast Ion Transport in Solids, ed. by P. Vashista, J. N. Mundy and G. K. Shenoy (New York: Elsevier North-Holland, Inc., 1979) p. 395.
4. R. Kikuchi and H. Sato, J. Chem. Phys. 55, 677 (1971); ibid, 55, 702 (1971).
5. C. Domb, Adv. in Phys. 34, 1 (1960).
6. G. S. Rushbrooke and H. I. Scions, Proc. Roy. Soc. A230, 74 (1955).
7. A. D. LeClaire in Mass Transport Phenomena in Ceramics, ed. by A. R. Cooper and A. H. Heuer (New York: Plenum Press, 1975) p. 17.
8. G. E. Murch and R. J. Thorn, Phil. Mag. 36, 529 (1977).
9. H. Sato, in Solid Electrolytes, Topics in Appl. Phys. 21, ed. by S. Geller (Berlin: Springer-Verlag, 1977) p. 3.
10. D. B. McWhan, S. J. Allen, J. P. Remeika and P. D. Dernier, Phys. Rev. Letters 35, 953 (1975).
11. J. R. Bates, G. M. Brown, T. Kaneda, W. E. Brundage, J. C. Wang and H. Engstrom, in Fast Ion Transport in Solids, ed. P. Vashishta, J. N. Mundy and G. K. Shenoy (New York: Elsevier North Holland, Inc., 1979) p. 261.
12. A. B. Kuper, D. Lazarus, J. R. Manning and C. T. Tomizuka, Phys. Rev. 104, 1536 (1956).

13. E. W. Elcock and C. W. McCombie, Phys. Rev. 109, 605 (1958).

14. I. Wynn Jones and L. J. Miles, Proc. Brit. Ceram. Soc. 19, 161 (1971).

15. W. L. Roth, General Electric Corporate Research and Development Report No. 74 CRD 054, March 1974.

16. M. Y. Hsieh and L. C. DeJonghe, J. Am. Ceram. Soc. 61[5-6], 185 (1978)

17. L. E. Davis, N. C. Macdonald, P. W. Palmberg, G. E. Rich, and R. E. Weber, "Handbook of Auger Electron Spectroscopy" (Physical Electronics Industries, Inc., 1972).

18. R. Ridgeway, A. Klein, and W. O'Leary, Trans. Electrochem. Soc. 70, 71 (1936).

19. J. B. Goodenough et.al., Semiannual Technical Report, Lincoln Laboratory, M.I.T., December 1974 (NTIS AD-A009 145).

20. J. B. Goodenough, H. Y-P Hong, and J. A. Kafalas, Mat. Res. Bull. 11, 203 (1976).

21. H. Y-P. Hong, J. A. Kafalas, and J. B. Goodenough, J. Solid State Chem. 9, 345 (1974).

22. W. S. Brower et.al., Mat. Res. Bull. 9, 1045 (1974).

23. J. L. Waring, R. S. Roth, H. S. Parker, and W. S. Brower, J. of Research 80A, 761 (1976).

24. R. S. Roth, W. S. Brower, H. S. Parker, D. B. Minor, and J. L. Waring, NASA Technical Report, Contract C-50821-C, NASA Cr-134869 (1975).

25. J. Singer, W. L. Fielder, H. E. Kautz, and J. S. Fordyce, J. Electrochem. Soc. 123, 614 (1976).

26. J. E. Bauerle, J. Phys. Chem. Solids 30, 2657 (1969).

27. H. Y-P. Hong, Mat. Res. Bull. 11, 173 (1976).

28. J. B. Goodenough, H. Y-P. Hong and J. A. Kafalas, Mat. Res. Bull. 11, 203 (1976).

29. M. L. Bayard and G. G. Barna, J. Electroanal. Chem. 91, 201 (1976).

30. U. von Alpen, M. F. Bell and W. Wichelhaus, Mat. Res. Bull. 14, 1317 (1979).

31. J. P. Boilot, J. P. Satanie, G. Desplanches and D. Le Potier, Mat. Res. Bull. 14, 1469 (1979).

32. D. C. Ginnings and T. E. Phipps, J. Am. Chem. Soc., 52, 1340 (1930).

33. B.J.H. Jackson and D. A. Young, J. Phys. Chem. Solids, 30, 1973 (1969).

34. R. M. Biefeld and R. T. Johnson, Jr., J. Solid State Chem. 29, 393 (1979).

35. R. D. Armstrong, T. Dickinson and P. Willis, J. Electroanal. Chem. 48, 47 (1973).

TABLE I Some physical properties of CaO-doped β"-alumina samples

wt% of CaO	Density ($g\ cm^{-3}$)	β" phase conversion	Bulk resistivity at 300°C(Ω-cm)	Remarks
0.05	3.15	83%	4.35	*
0.2	3.23	80%	6.45	*
0.5	3.22	69.5%	12.5	*
0.7	3.21	78.9%	17.5	*
1.0	3.21	85.3%	33.3	*

Remarks:

* All the samples were sintered at 1585°C for 7 min. and post-sinter annealed at 1400°C for 4h.

* All showed duplex structure.

TABLE II Various methods of fabricating primitive cubic and body-centered cubic metal antimonates.

STARTING MATERIAL	PROCESSING	RESULTS
$KSbO_3$(ilmenite)	20kb, 700°C	$KSbO_3$(bcc)
$KSbO_3$(bcc)	Fired at 1200°C, 16 hrs.	$KSbO_3$(Prim. cubic)
$K_2CO_3+Sb_2O_4$	Fired at 1200°C	$KSbO_3$(ilmenite)
$K_2CO_3+Sb_2O_4$	Doped with two mole % B_2O_3, fired at 1200°C	$K_{1.17-x}SbO_{3-x}(OH)_{2+x}$ (prim. cubic)
$K_2CO_3+Sb_2O_4$ (slightly K_2O deficient)	Fired at 1200°C	$K_{1.17-x}SbO_{3-x}(OH)_{2+x}$ (prim. cubic)
$KSbO_3$(ilmenite) + excess KF	Fired at 1000°C	$KSbO_3\cdot\frac{1}{6}(KF)$ (bcc)
	ION EXCHANGE	
$KSbO_3$ or $KSbO_3\cdot\frac{1}{6}(KF)$ (bcc)	Aqueous or molten MNO_3(M=Li,Na,Rb,Tl,Ag) exchange reversible except for Ag.	$MSbO_3\cdot\frac{1}{6}(MF)$ (bcc)
$K_{1.17-x}SbO_{3-x}(OH)_{2+x}$ (prim. cubic)	Aqueous $NaNO_3$, 100°C	$Na_{1.17-x}SbO_{3-x}(OH)_{2+x}$ (bcc)

TABLE III Experimentally determined values for the equivalent circuit elements of Figure 20

Geometric Capacitance, C_g	2×10^{-10} F/cm^2
Double Layer Capacitance, C_{dl}	4×10^{-6} F/cm^2
Bulk Resistance, R_b	$R_b = R_oT \exp(E_a/kT)$ where $R_o = 1 \times 10^{-5}$ ohms $E_a = 0.49$ eV
Interfacial Impedance, Z_i	f(T) (undetermined function of temperature which may include an activated process, $E_a = 0.36$ eV)

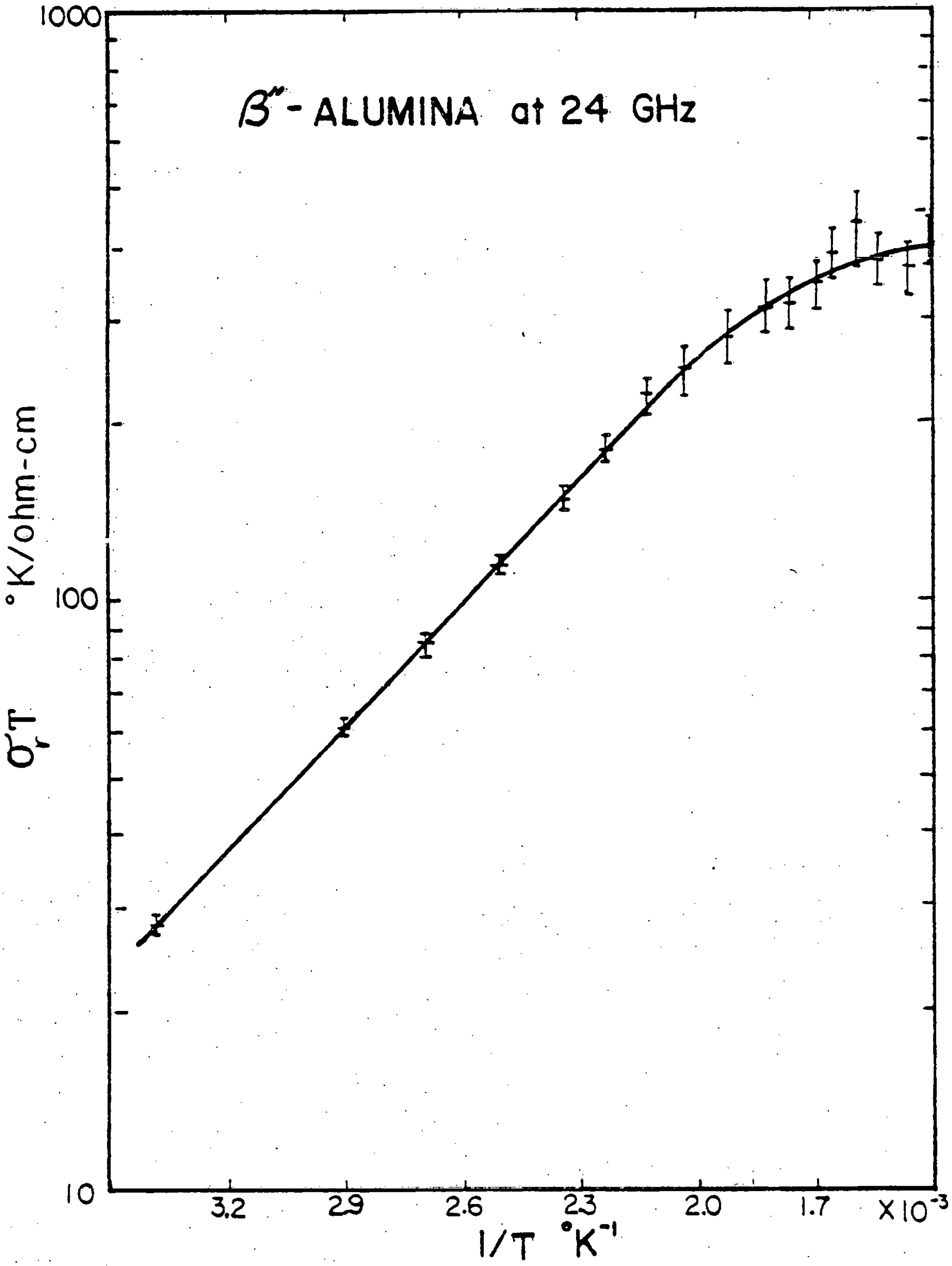

Figure 1. Arrhenius plot of the real part of the ionic conductivity, measured at 24 GHz, for polycrystalline sodium β''-alumina.

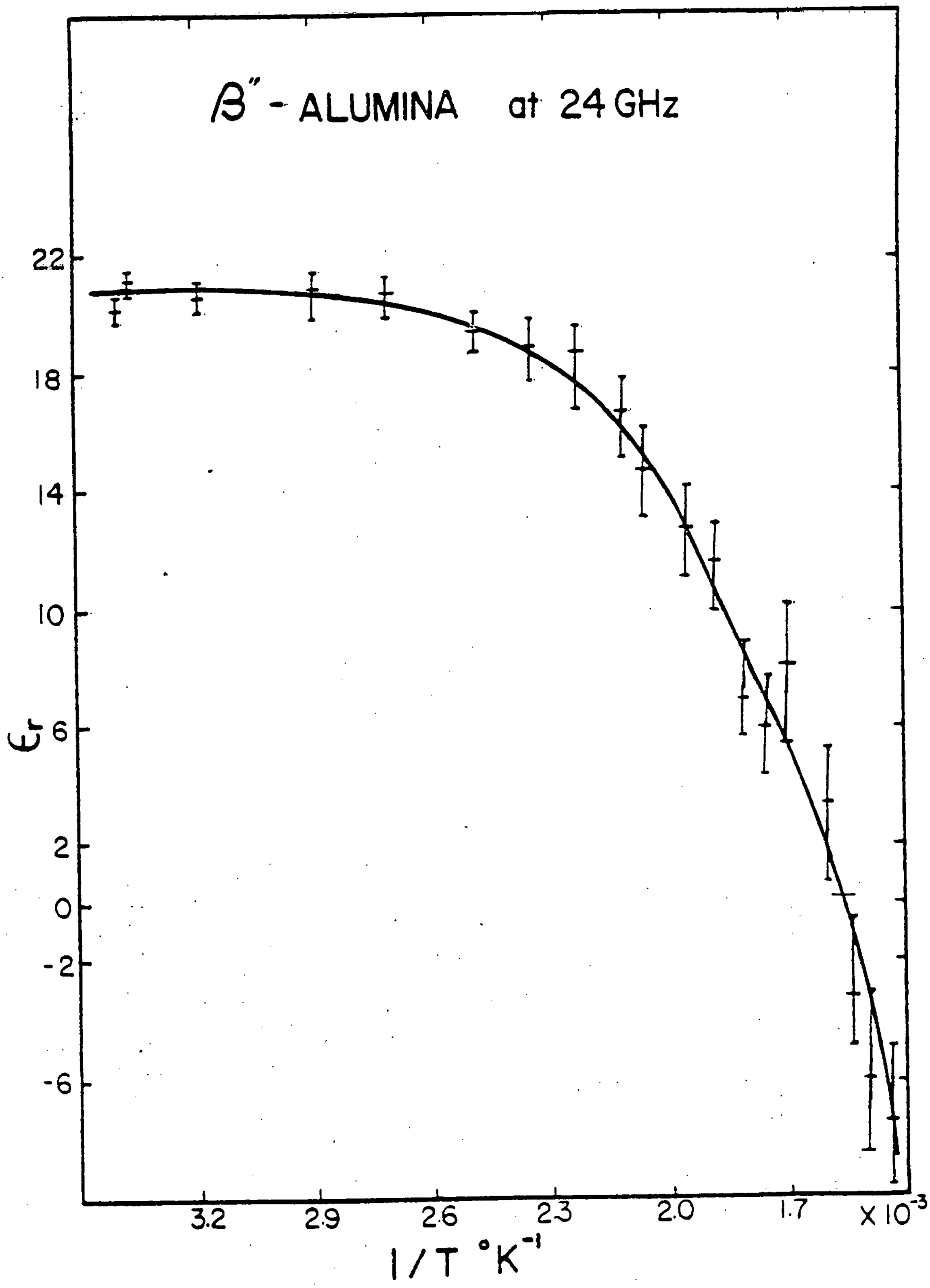

Figure 2. Plot of real part of the dielectric constant versus the reciprocal of the absolute temperature for sodium β''-alumina measured at 24 GHz.

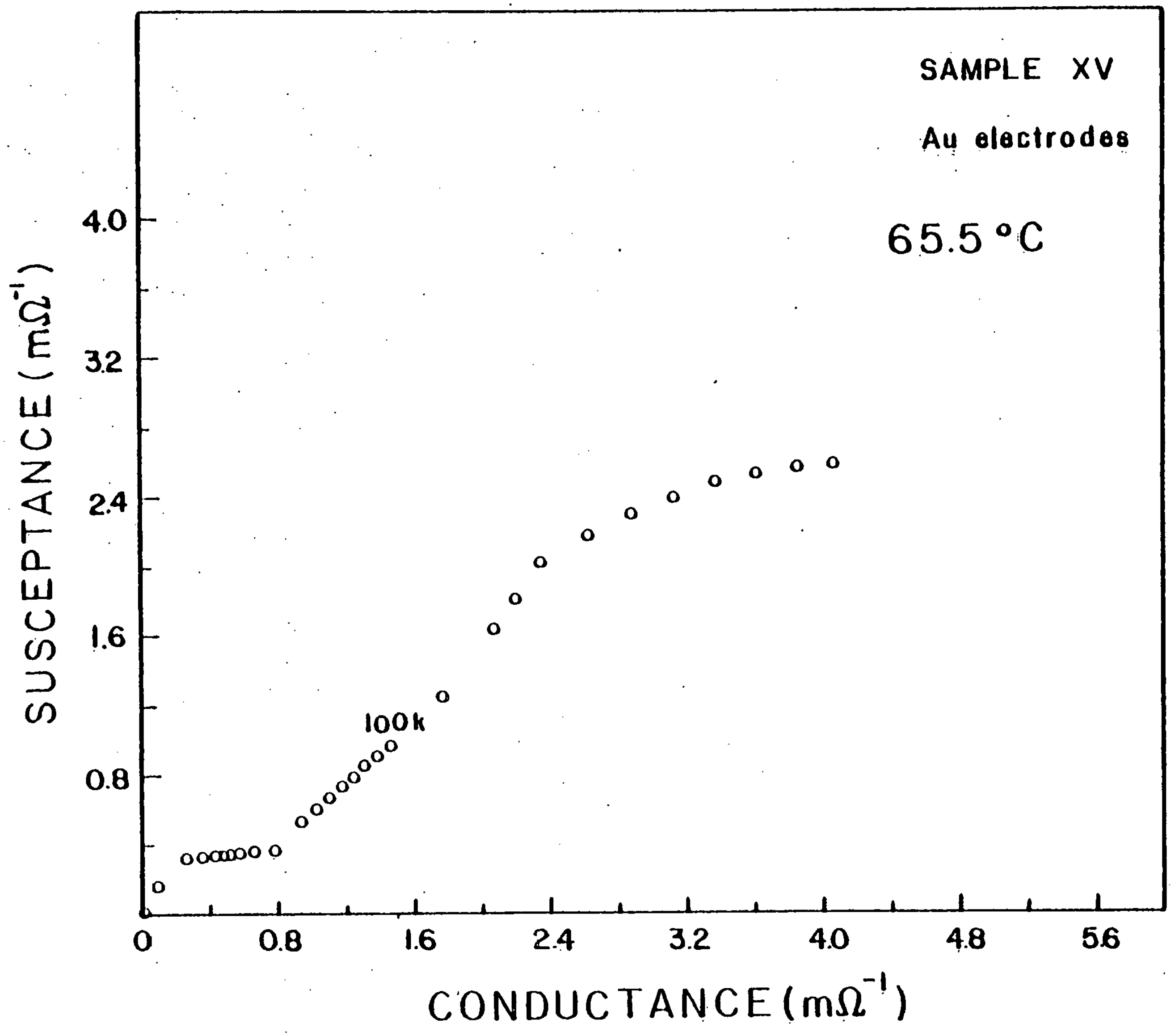

Figure 3. Typical B vs. G plot at 65.5°C for Na β''-alumina sample doped with 0.7 wt% CaO.

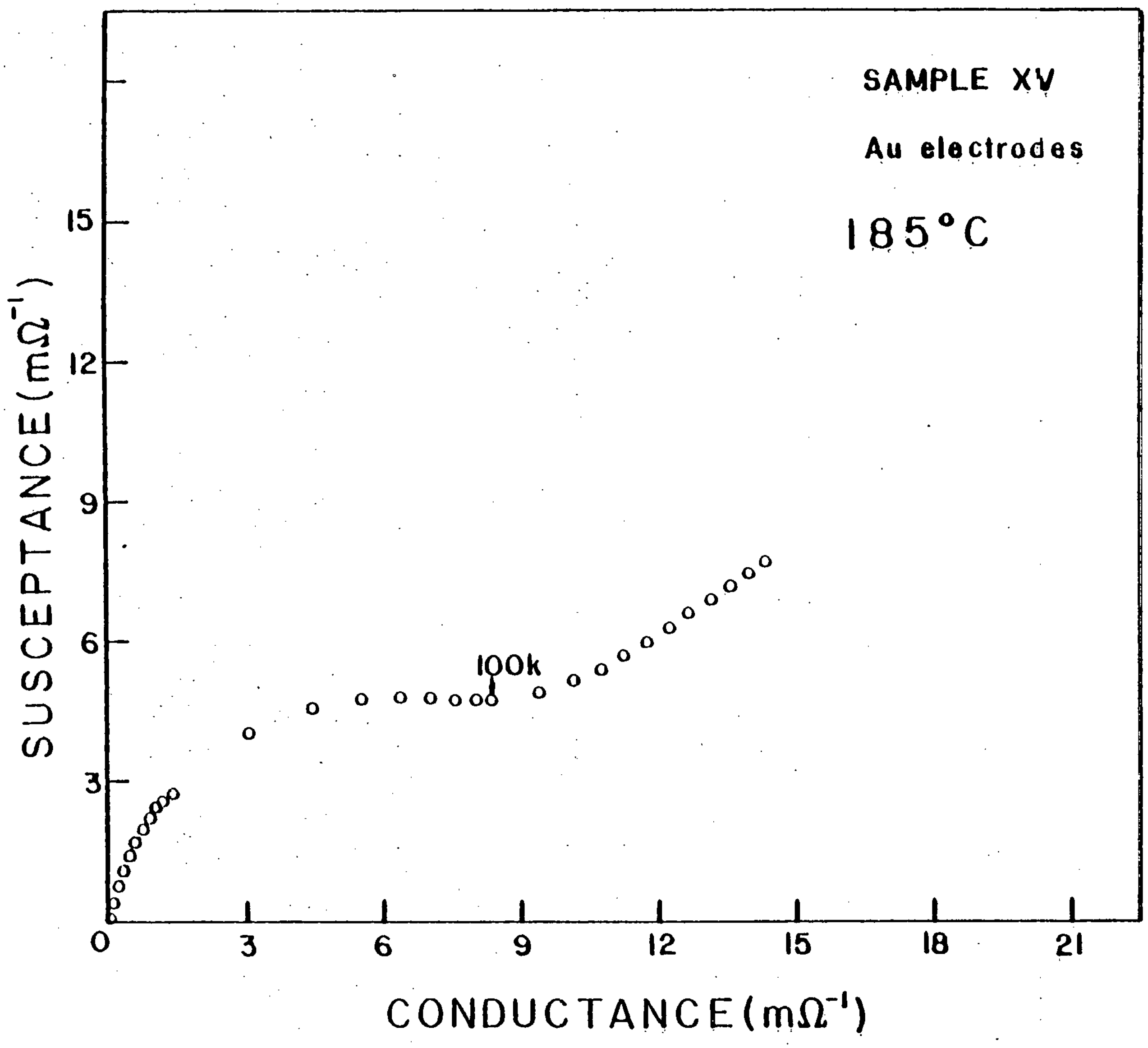

Figure 4. Typical B vs. G plot at 185°C for Na β''-alumina sample doped with 0.7 wt% CaO.

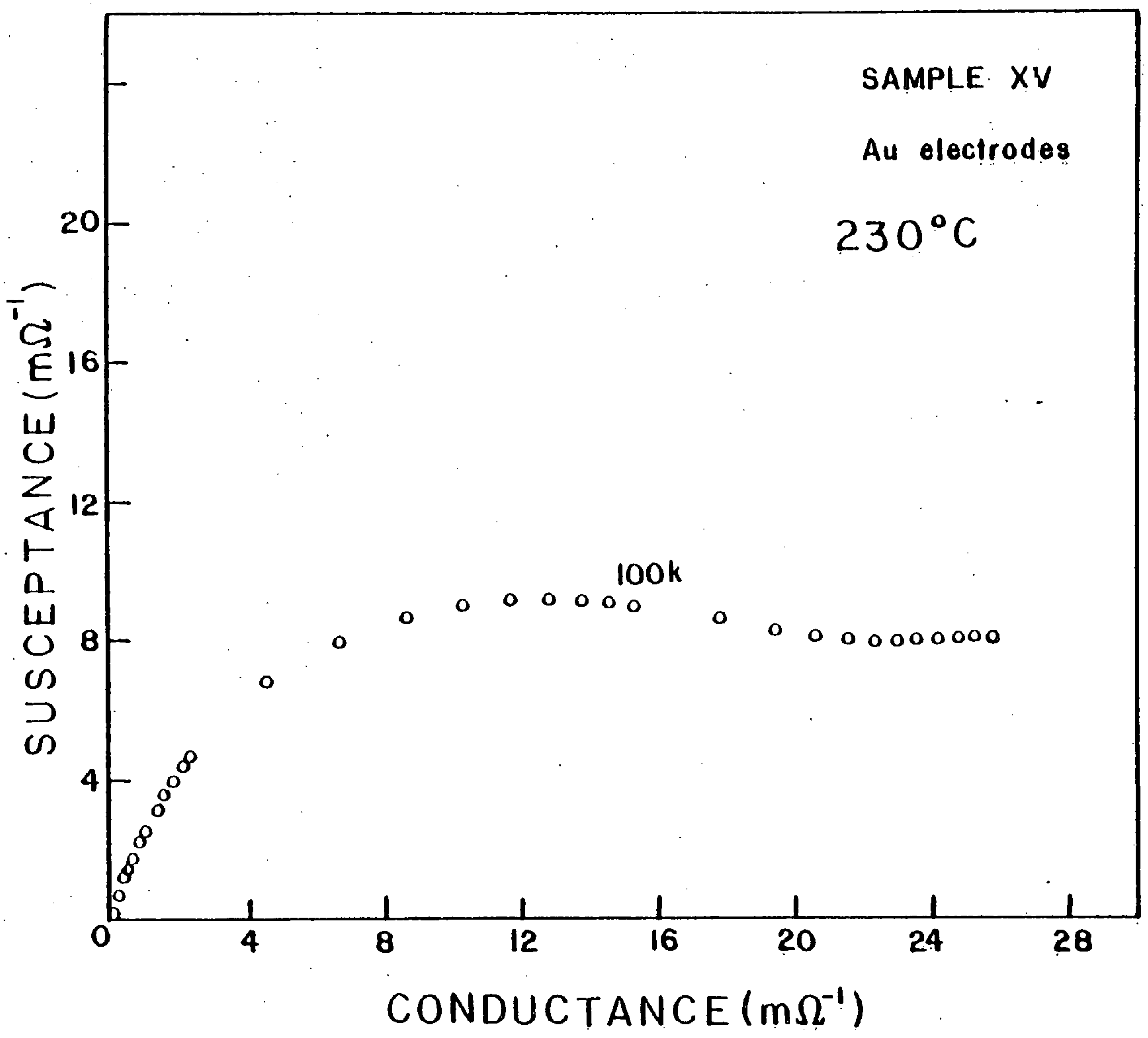

Figure 5. Typical B vs. G plot at 230°C for Na β"-alumina sample doped with 0.7 wt% CaO.

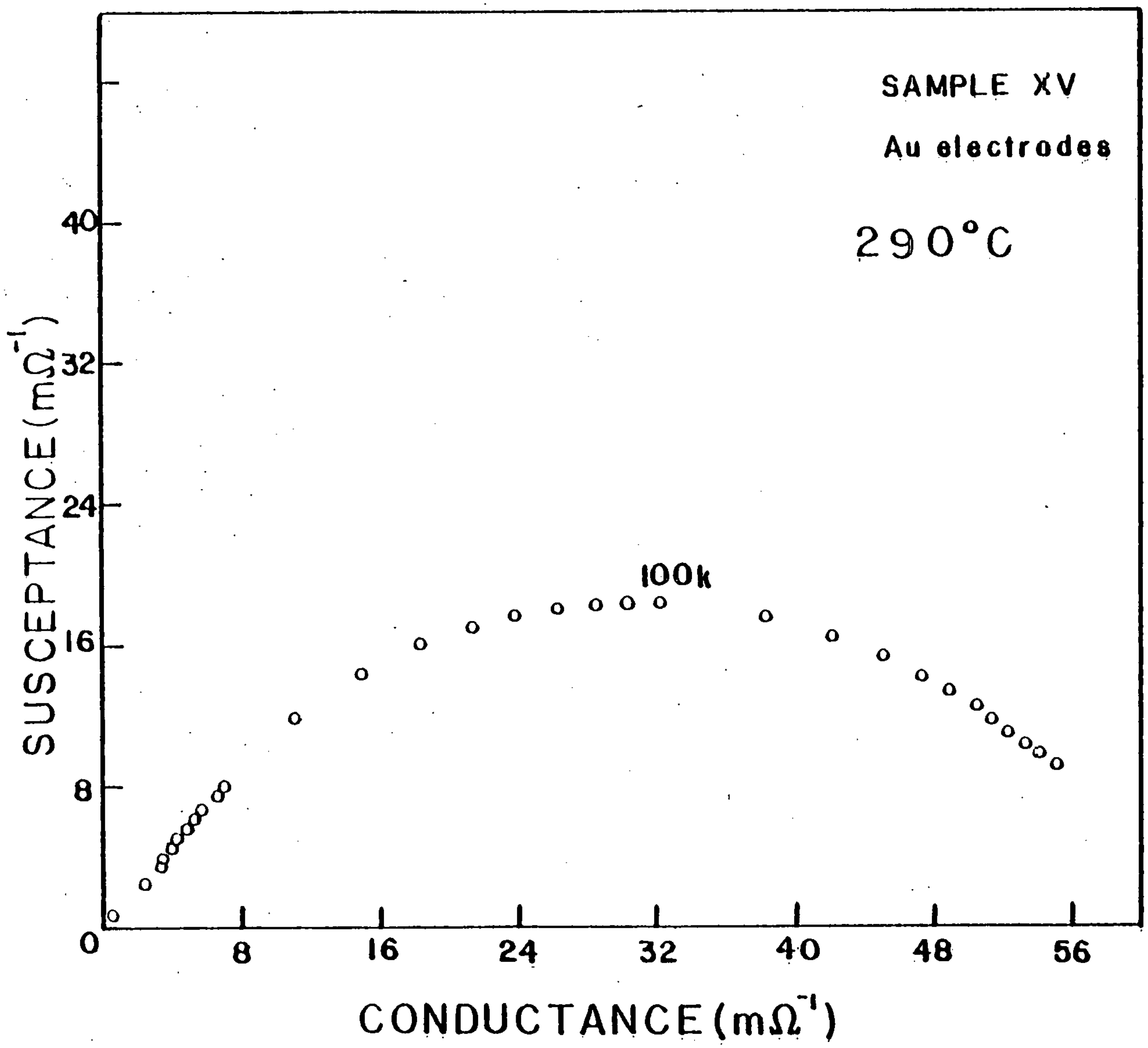

[illegible] plot at 290°C for Na β''-alumina sample doped with 0.7 wt% CaO

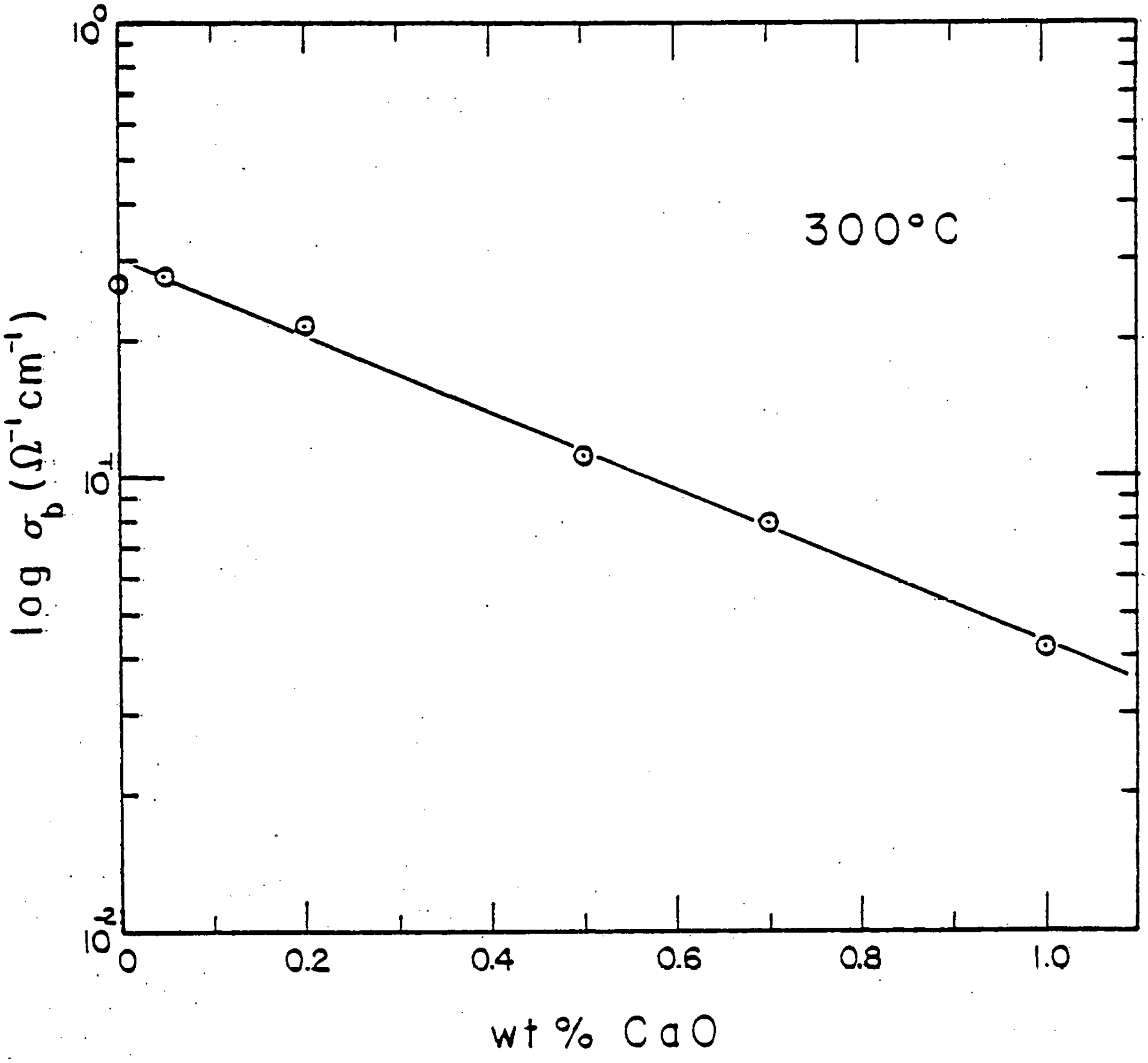

Figure 7. Isothermal conductivity-composition plot of bulk conductivity at 300°C for CaO-doped Na β''-alumina samples.

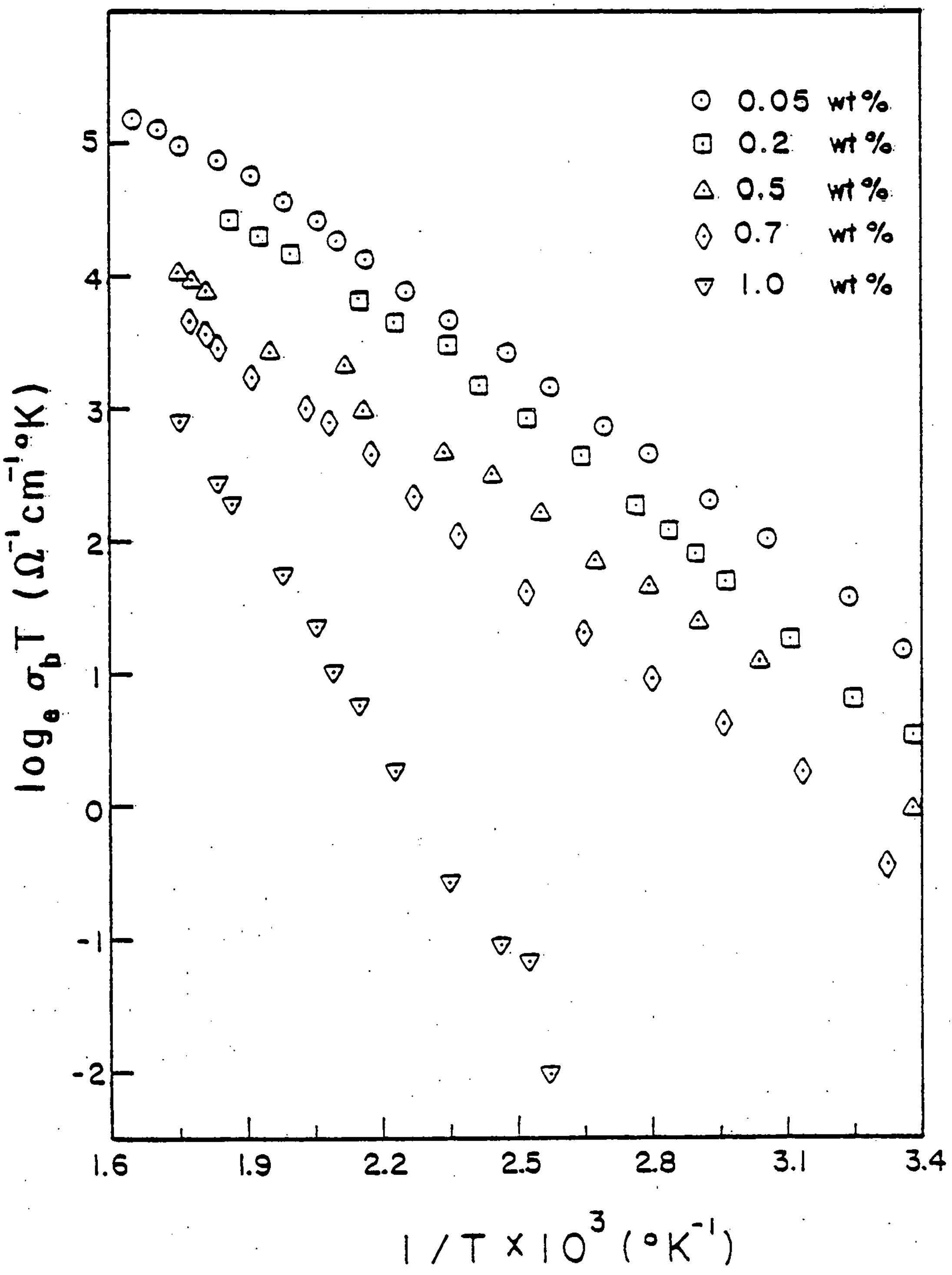

Figure 8. $\ln \sigma_b T$ vs. T^{-1} plots for various CaO-doped Na β''-alumina samples.

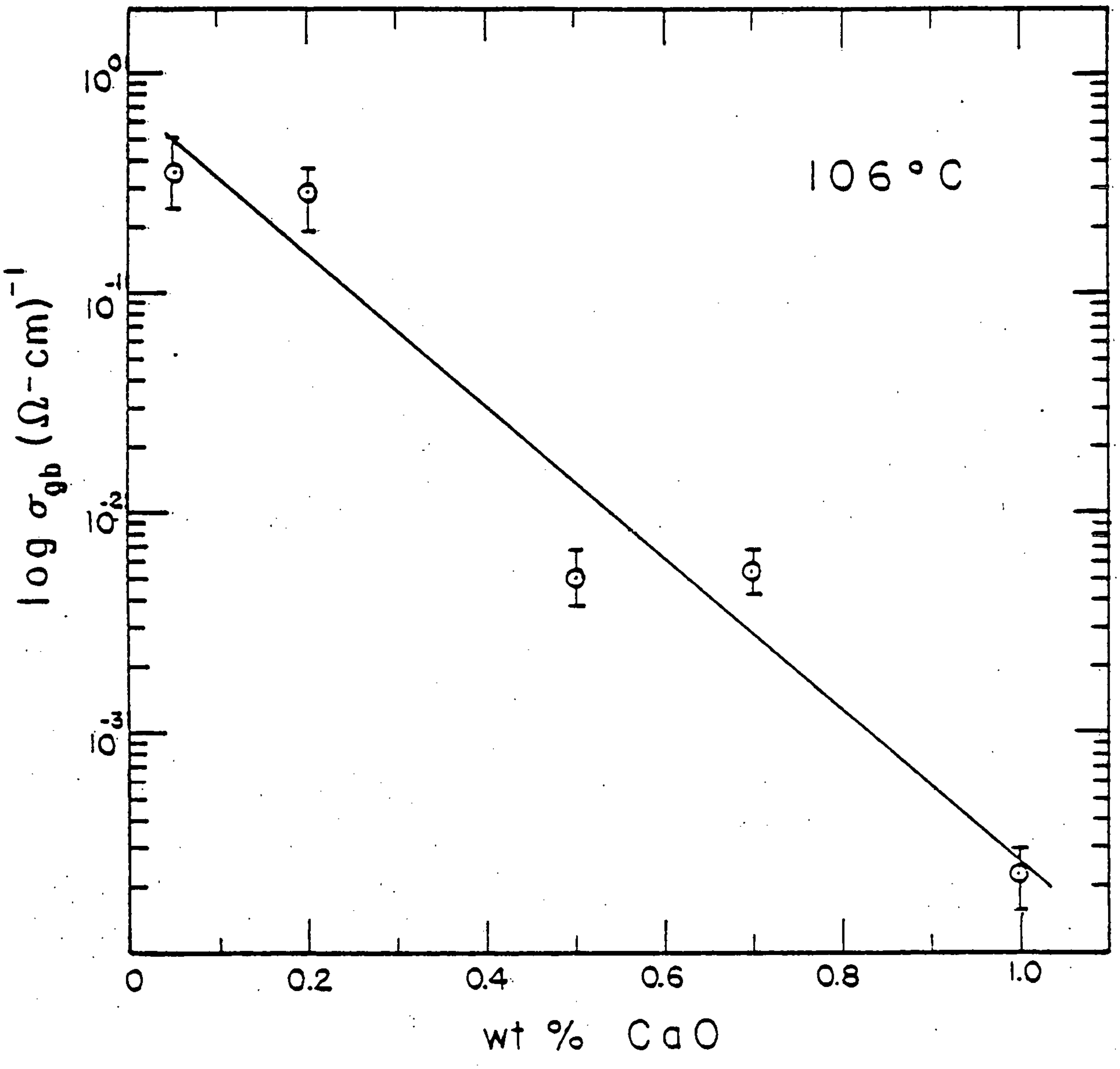

Figure 9. Isothermal conductivity-composition plot of grain boundary conductivity at 106°C for CaO-doped Na β''-alumina samples.

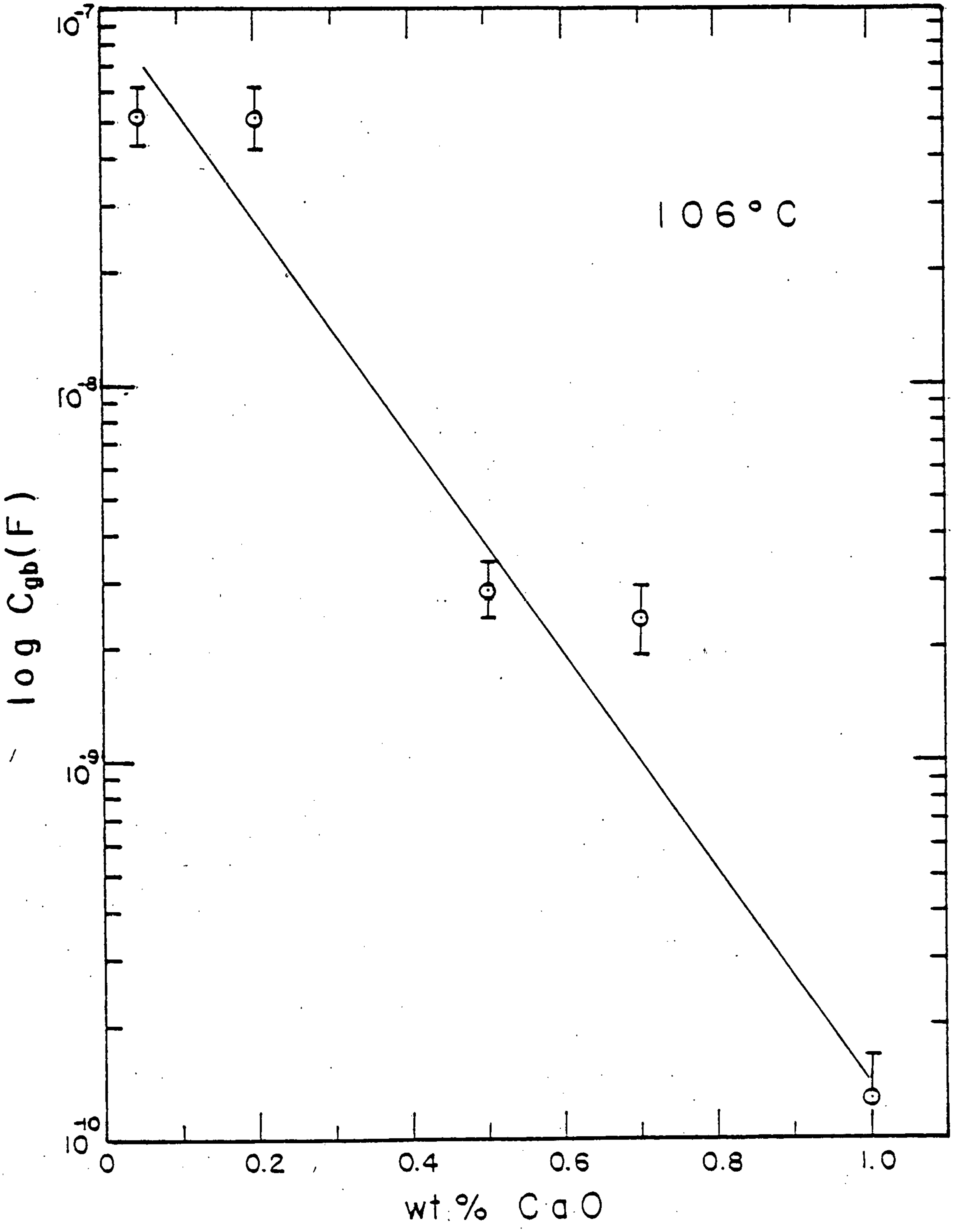

Figure 10. Isothermal grain boundary capacitance-composition plot for the CaO-doped Na β"-alumina samples at 106°C.

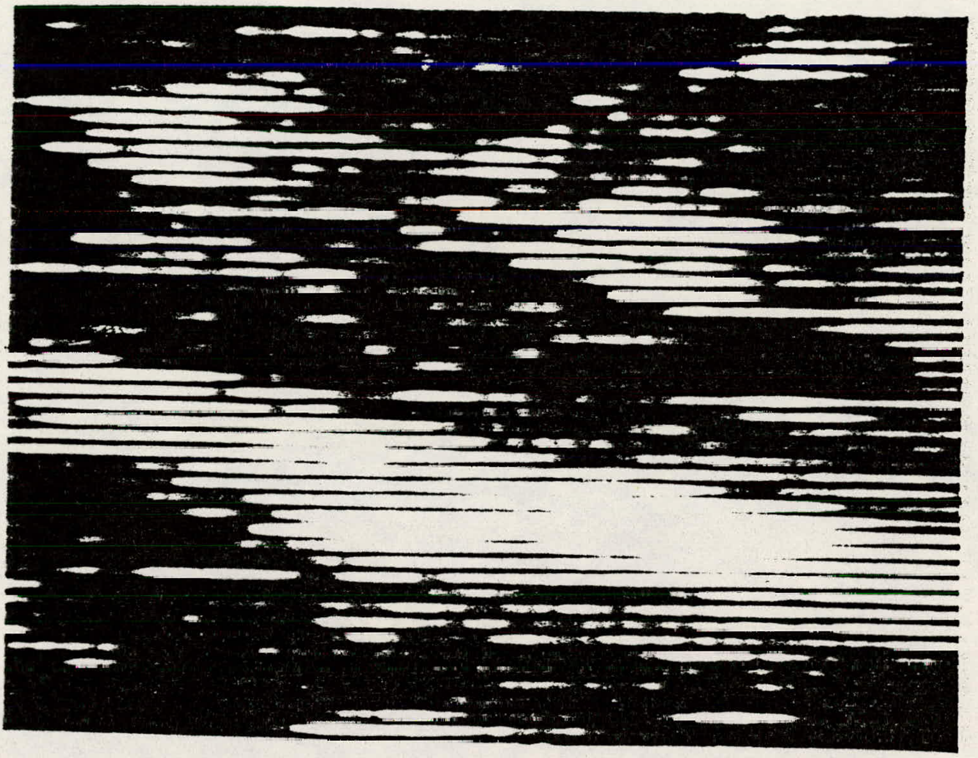

Figure 11. An Auger mapping for the element Ca of a Na β''-alumina sample doped with 1 wt% CaO.

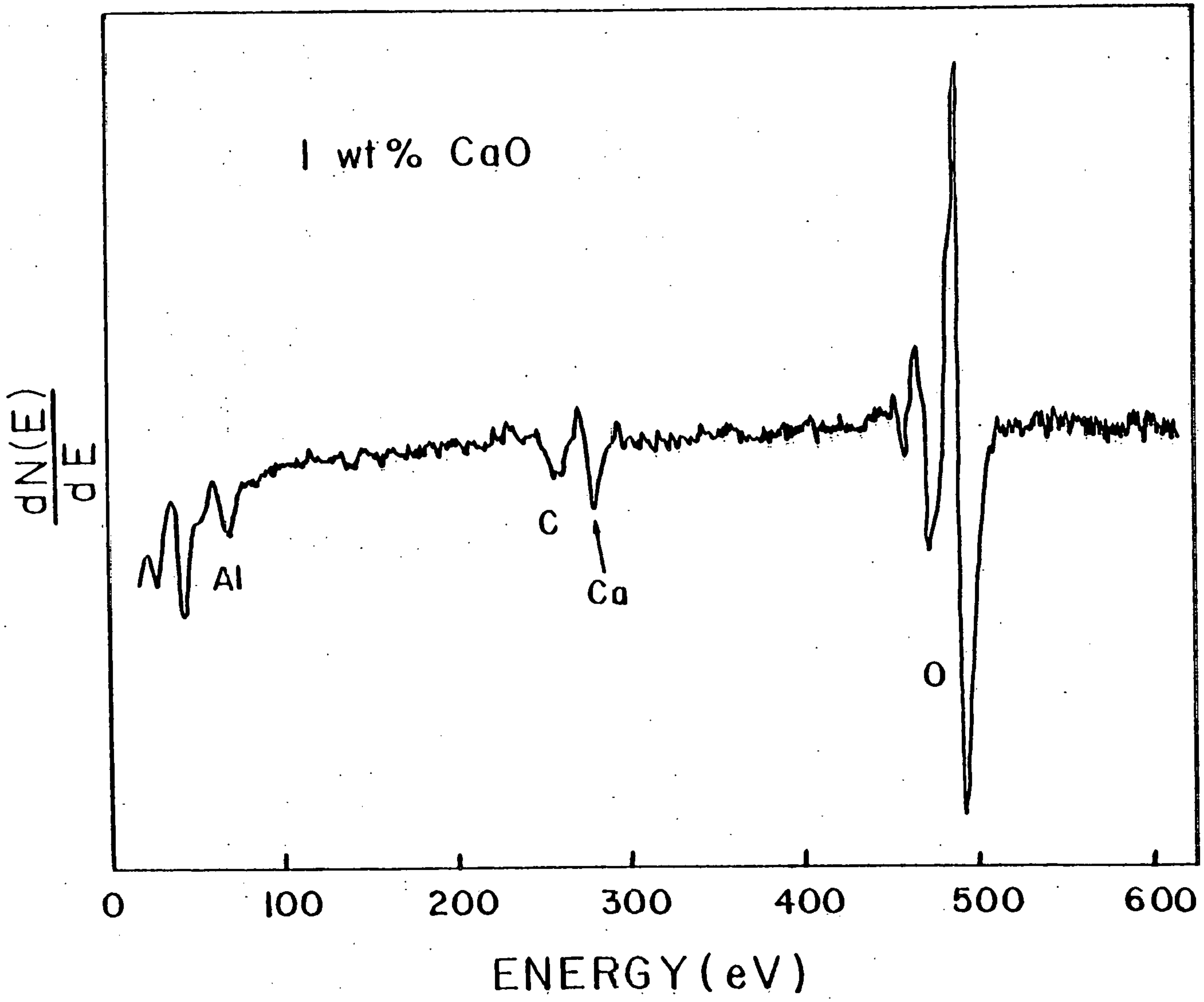

Figure 12. Auger spectrum for a Na β"-alumina sample doped with 1 wt% CaO.

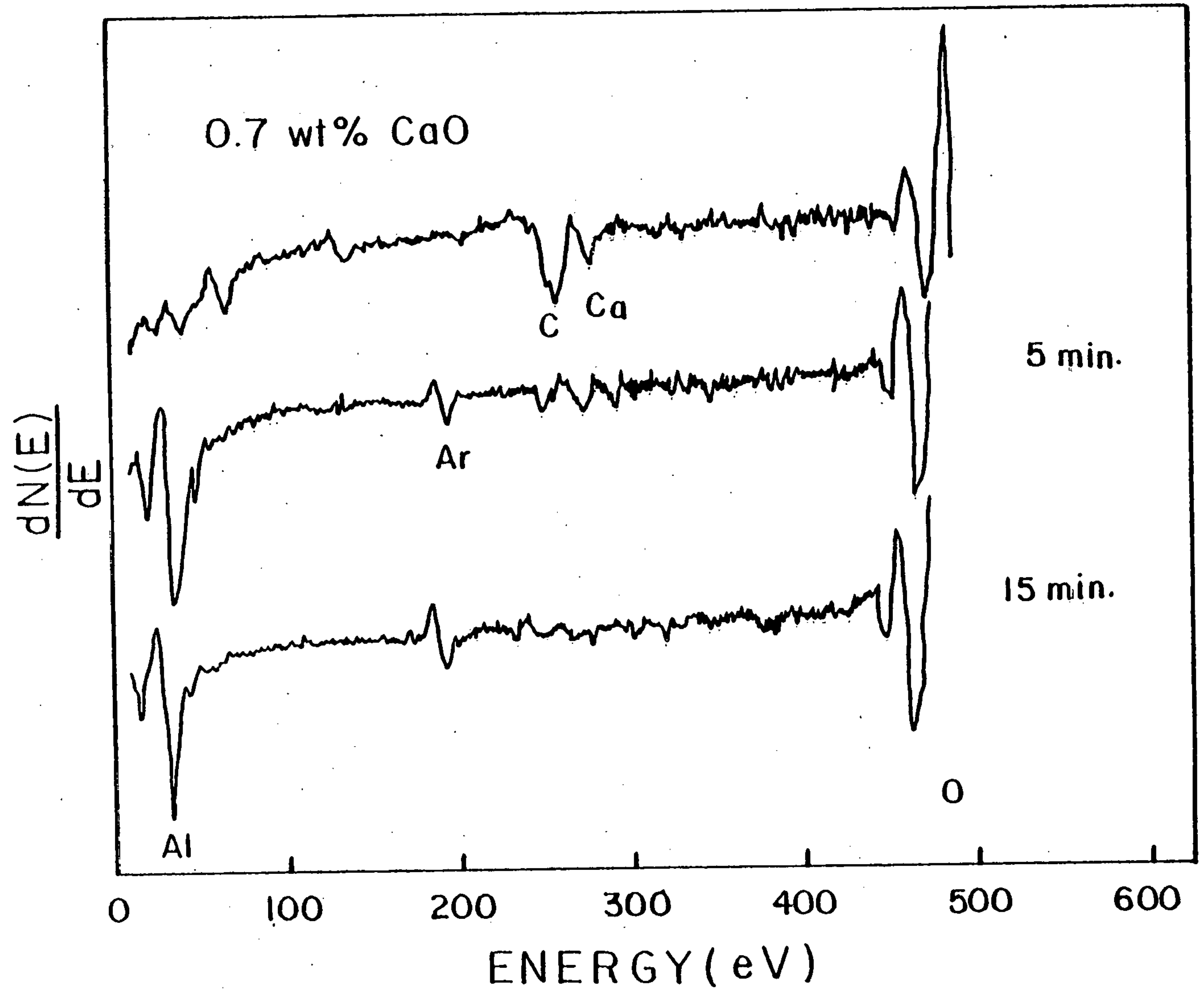

Figure 13. Auger spectra for a Na β''-alumina sample doped with 0.7 wt% CaO : (a) as-cut surface (b) after 5 min. argon ion-milling at 2 kV and 25 mA (c) after 15 min. argon ion-milling at 2 kV and 25 mA.

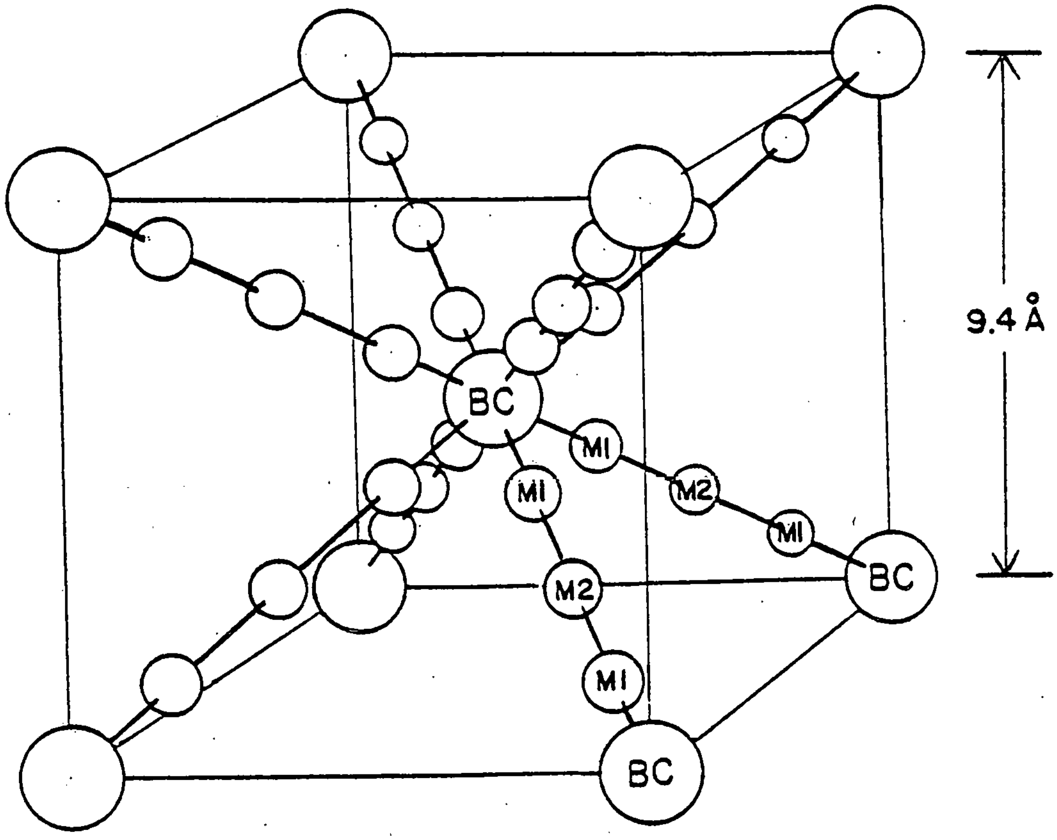

FIGURE 14. Schematic representation of 111 tunnels in sodium (potassium) antimonate. Cations reside at sites labled M1 and M2. Tunnel intersection sites are labled BC. Fluorine or hydroxyl ions reside at BC sites in the stabilized antimonates.

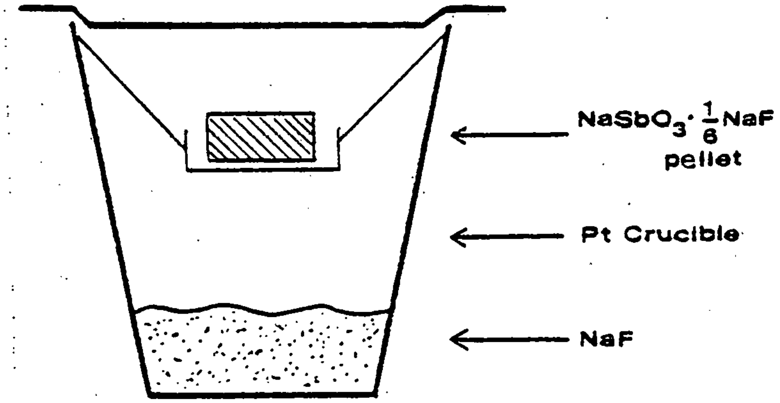

FIGURE 15. Sample arrangement for single crystal growth.

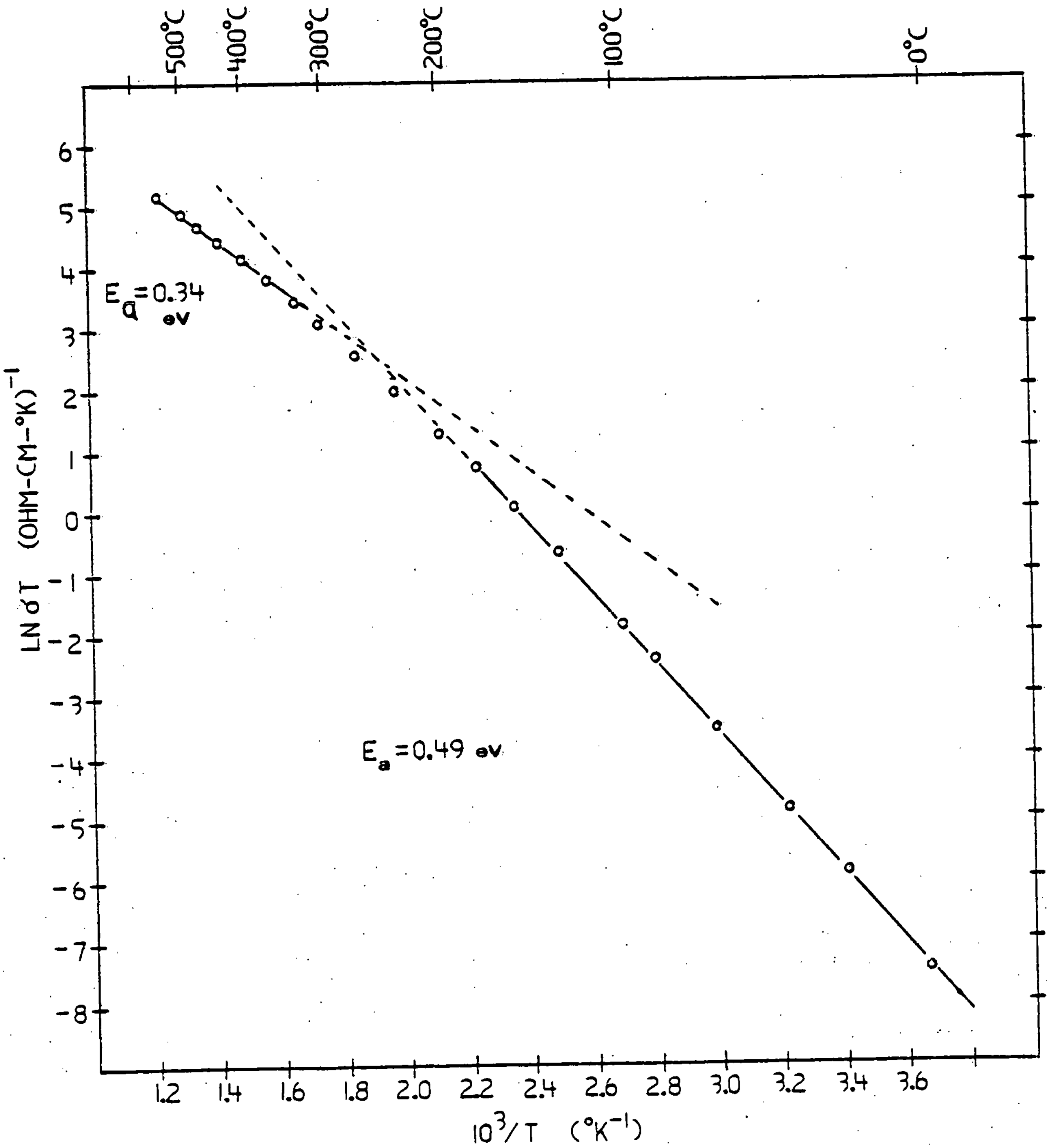

FIGURE 16. Arrhenius plot of data collected on a single crystal of $NaSbO_3 \cdot 1/6(NaF)$. Complex plane analysis was used.

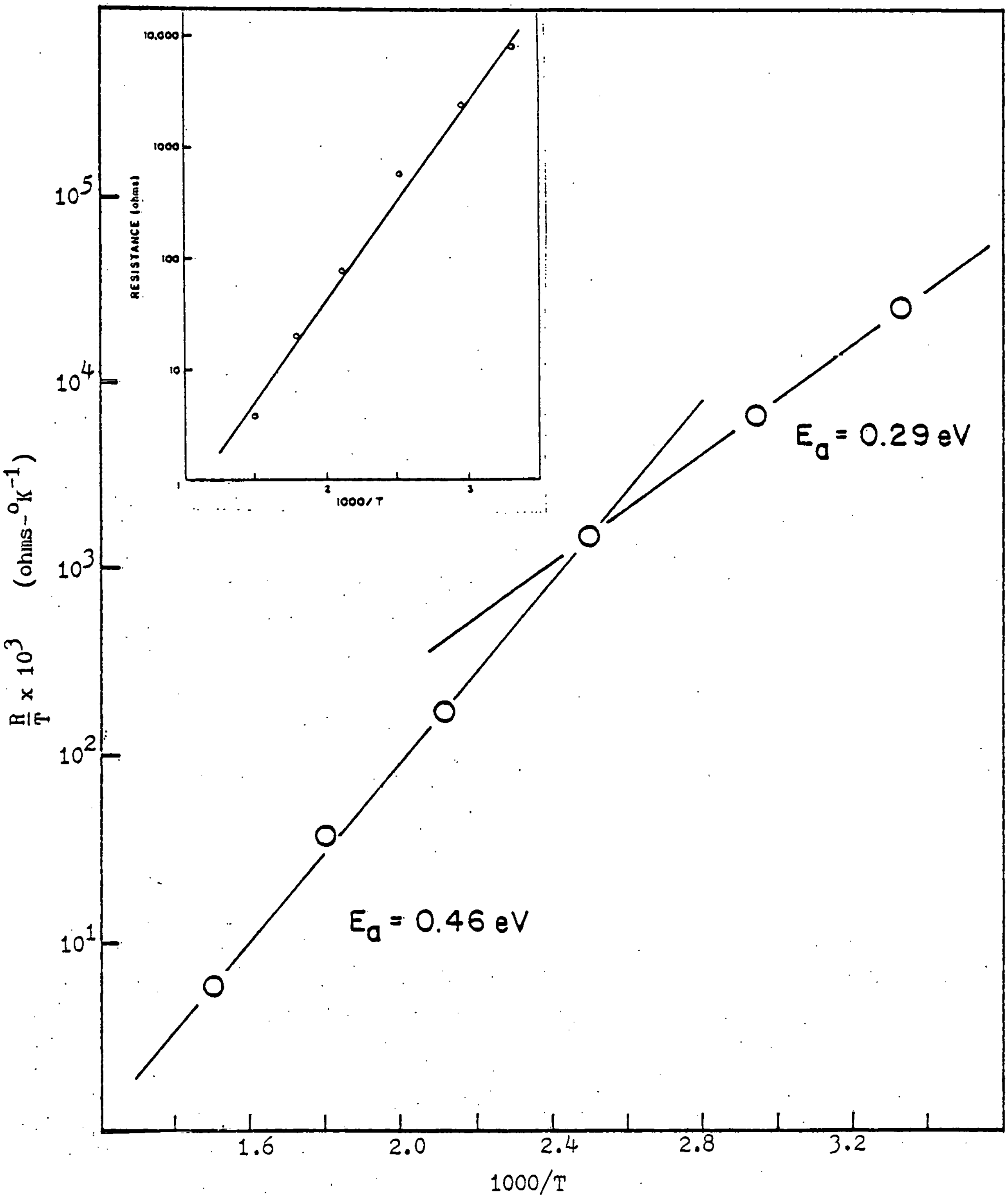

FIGURE 17. Replot of Goodenough et. al. data for $NaSbO_3$ · 1/6 (NaF) polycrystalline sample with graphite electrodes at 1kHz. Insert is original data.

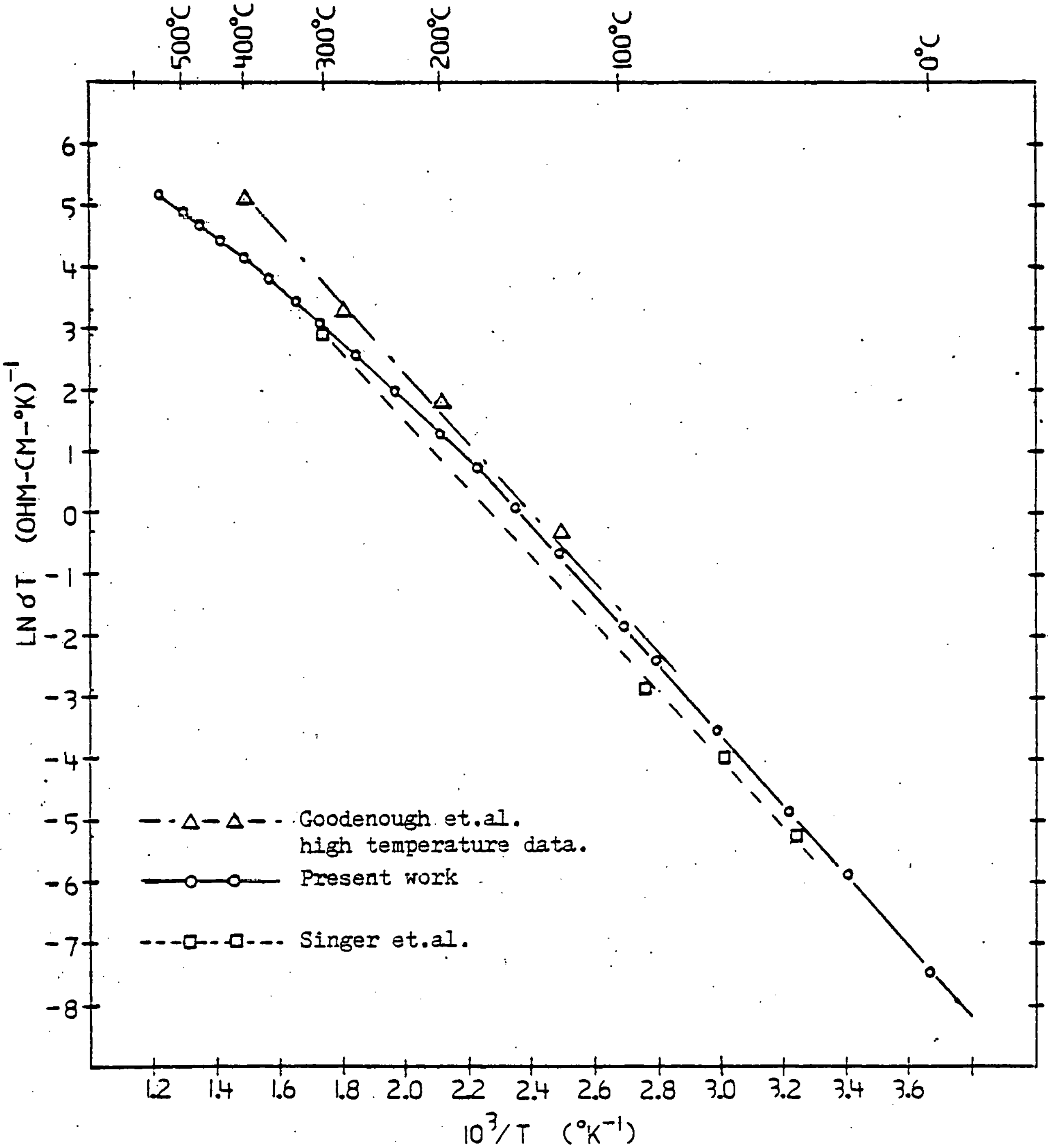

FIGURE 18. Comparison of the results of the present work with those of Goodenough et.al. and Singer et.al.

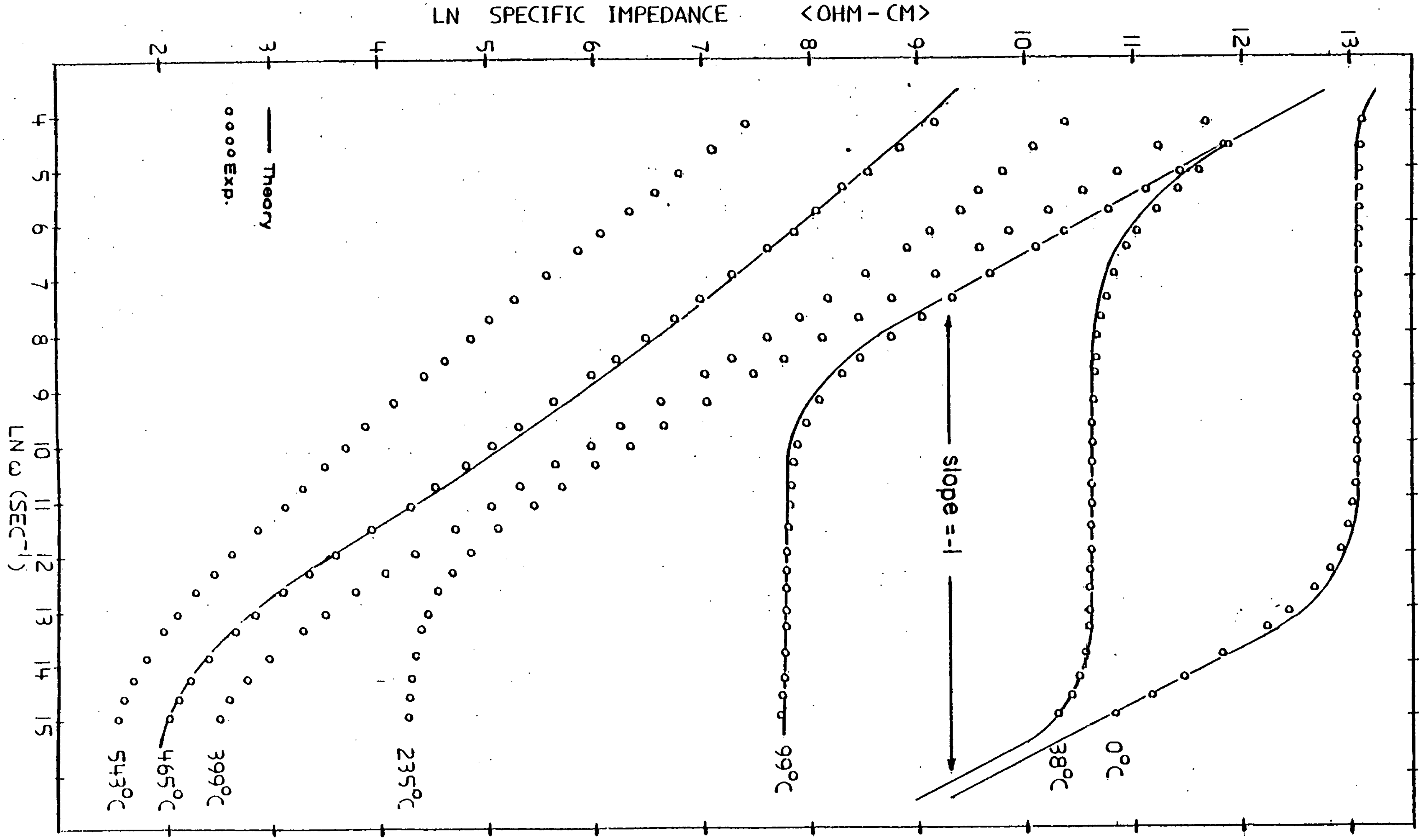

FIGURE **19.** Bode plot of data collected on a single crystal of $NaSbO_3 \cdot 1/6(NaF)$ using graphite electodes. Solid lines derived from equivalent circuit shown in text.

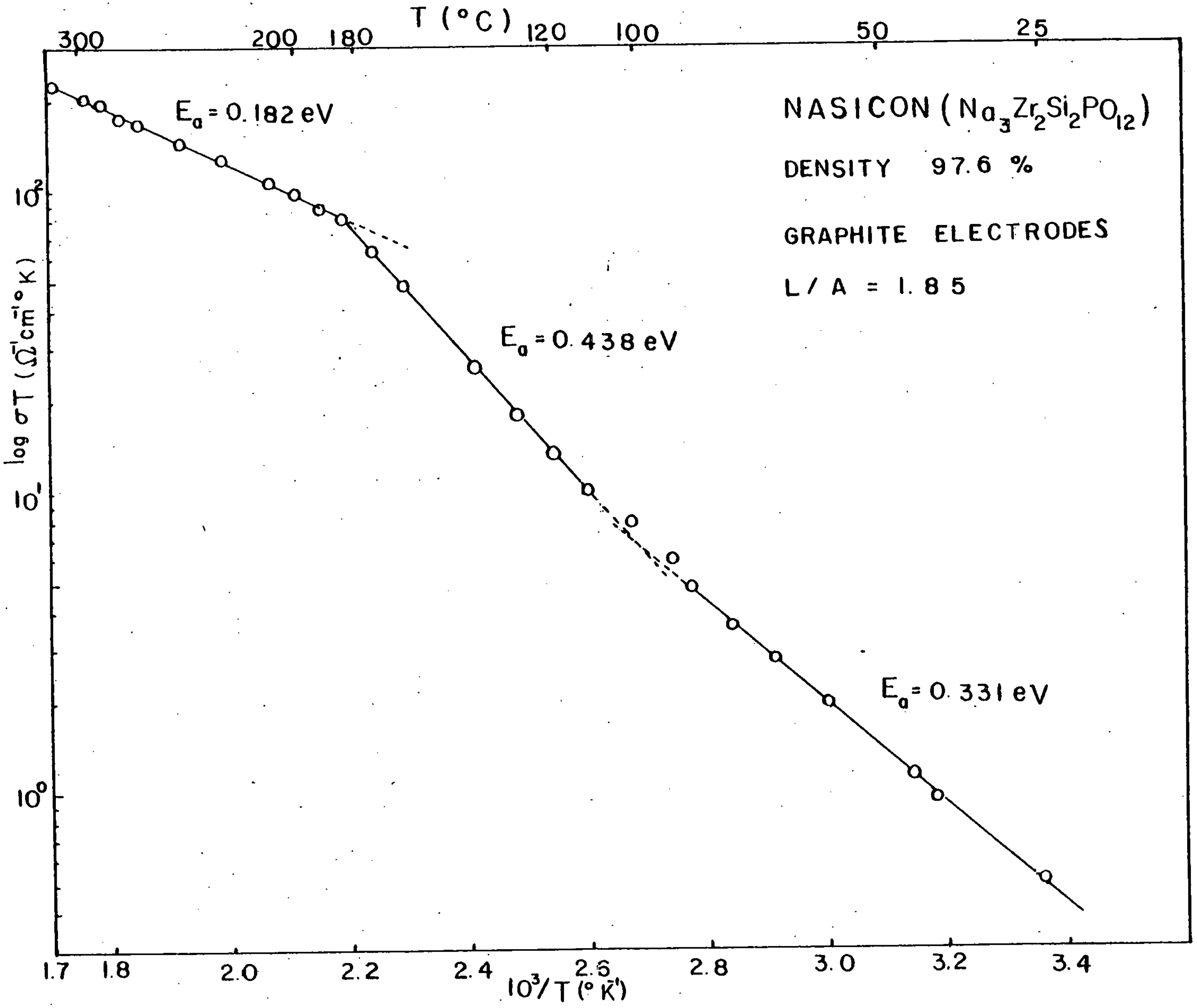

Figure 21. Arrhenius plot of the ionic conductivity of polycrystalline NASICON.

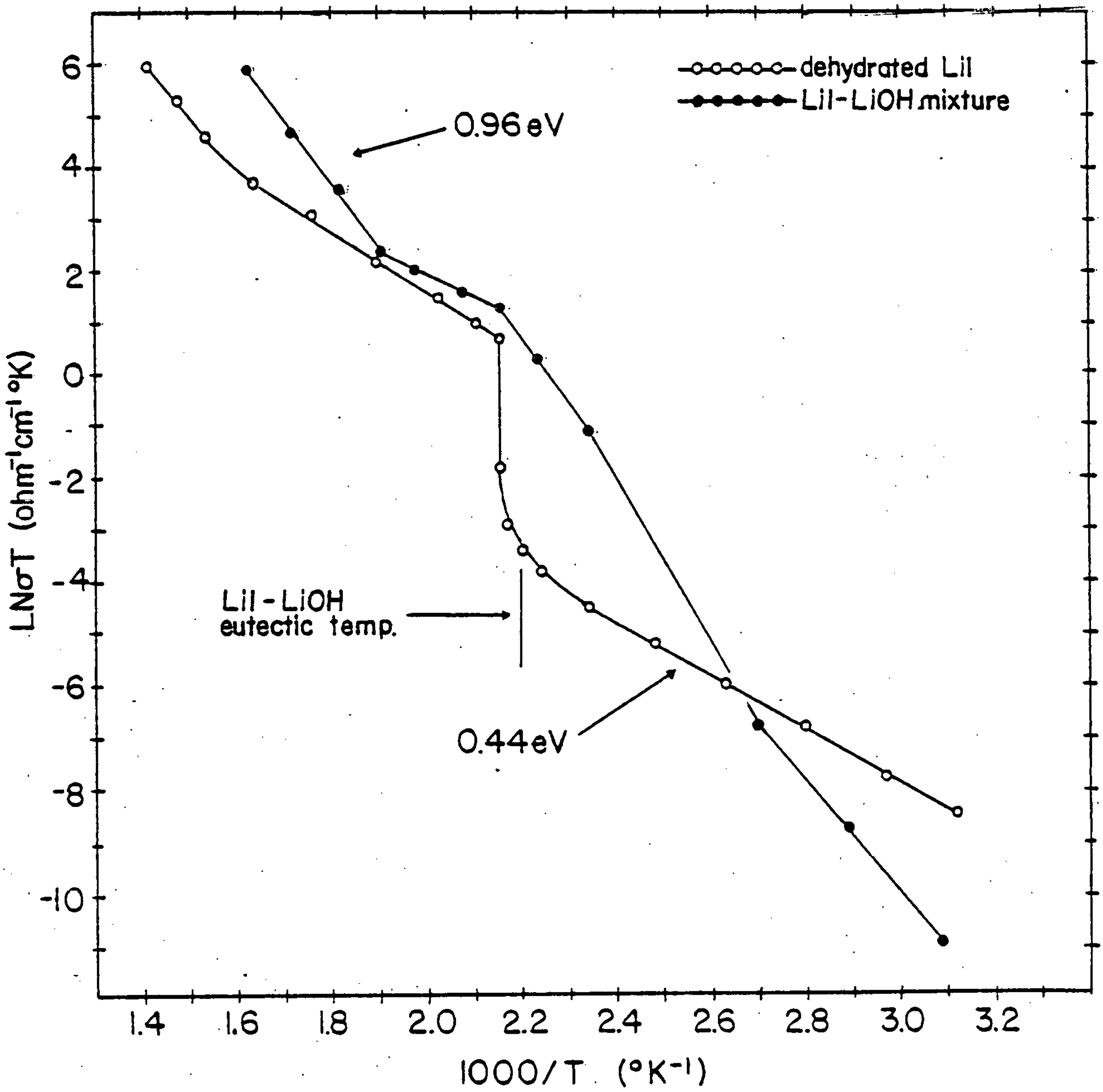

Figure 22. Arrhenius plots of the ionic conductivity of dehydrated LiI and a LiI + LiOH mixture.

Time Devoted to Project by Principal Investigator

The principal investigator, Donald H. Whitmore, has devoted 12% of his time during the academic year (April 1, 1979 - June 14, 1979 and September 15, 1979 to December 31, 1979) and nearly 2 full-time summer months (summer of 1979) to this project. He will continue to devote 12% of his time to this project during the remaining period of the present contract January 1, 1980 to March 31, 1981.

Publications and Talks on DOE Contract EY-76-S-02-2564 during 1979

Published:

W. Jakubowski and D. H. Whitmore, "Analysis of Electrolyte Polarization in Sodium β''-alumina by a Complex Admittance Method," J. Am. Ceramic Soc. 62, 321 (1979).

D. F. Shriver, M. A. Ratner, R. Ammlung, J. McComber, and D. H. Whitmore, "Indium (I) and Thallium (I) Transport in Halide Lattices," Proc. Int. Conf. on Fast Ion Transport in Solids, ed. by J. N. Mundy and P. Vashishta (North-Holland, New York, 1979) p. 521.

Awaiting Publication:

J. Ni, D. H. Whitmore and J. Baker, "An Automatic Frequency Response Analyzer for Impedance Measurements on Fast Ion Conductors," - to be published in Rev. Sci. Instru. (1980).

Manuscripts in Progress:

W. Bogusz and D. H. Whitmore, "Mechanisms of Sodium Ion Conduction in Single Crystal β''-alumina."

J. B. Phipps and D. H. Whitmore, "Model for Enhanced Cationic Mobility in Solid Electrolytes Containing a Dispersed Second Phase."

Invited Talk:

"Superionic Conductors: Fact or Fiction," University of Notre Dame, Dept. of Materials Science, Notre Dame, Indiana, February 23, 1979.